New families of vortex patch equilibria for the two-dimensional Euler equations

B. B. Xue, E. R. Johnson, and N. R. McDonald

Citation: Physics of Fluids **29**, 123602 (2017);
View online: https://doi.org/10.1063/1.5009536
View Table of Contents: http://aip.scitation.org/toc/phf/29/12
Published by the American Institute of Physics

New families of vortex patch equilibria for the two-dimensional Euler equations

B. B. Xue,[a] E. R. Johnson,[b] and N. R. McDonald[c]
Department of Mathematics, University College London, London WC1E 6BT, United Kingdom

(Received 17 October 2017; accepted 9 November 2017; published online 11 December 2017)

Various modified forms of contour dynamics are used to compute multipolar vortex equilibria, i.e., configurations of constant vorticity patches which are invariant in a steady rotating frame. There are two distinct solution families for "$N + 1$" point vortex-vortex patch equilibria in which a finite-area central patch is surrounded by N identical point vortices: one with the central patch having opposite-signed vorticity and the other having same-signed vorticity to the satellite vortices. Each solution family exhibits limiting states beyond which no equilibria can be found. At the limiting state, the central patch of a same-signed equilibrium acquires N corners on its boundary. The limiting states of the opposite-signed equilibria have cusp-like behaviour on the boundary of the central patch. Linear stability analysis reveals that the central patch is most linearly unstable as it approaches the limiting states. For equilibria comprising a central patch surrounded by N identical finite-area satellite patches, again two distinct families of solutions exist: one with the central patch and satellite patches having the same-signed vorticity and the other in which they are opposite-signed. In each family, there are two limiting behaviours in which either the central patch or the satellite patches develop corners or cusps. Streamline plots and time-dependent simulations indicate that opposite-signed multipolar equilibria are robust structures and same-signed equilibria are generally less stable. Streamlines also reveal stable and unstable (saddle point) stagnation points, indicating the existence of new equilibria in which additional patches of vorticity are "grown" at the stagnation points. Examples of such equilibria are computed, and a general numerical routine is briefly described for finding even more complex finite-area equilibria. Finally, new nested polygonal vortex equilibria consisting of two sets of polygonally arranged vortex patches (named "$N + N$" equilibria here) are computed for two distinct cases: one with the corners of the polygons aligned with each other and the other when they are staggered. Various limiting states are computed for these equilibria. Time-dependent simulations reveal that the aligned equilibria are susceptible to instability, while the staggered equilibria survive a relatively long time. In some parameter regimes, following instability, these structures evolve into known structures such as "$N + 1$" multipolar vortex equilibria and N-polygon co-rotating equilibria. https://doi.org/10.1063/1.5009536

I. INTRODUCTION

Arising from studies of magnetism and plasma physics, the well-known equilibria of identical point vortices arranged at the vertices of a polygon[1] which rotate steadily about the polygon's centre without change of shape have inspired many subsequent studies and the search for new equilibria involving point vortices of arbitrary strengths along with their stability analysis.[2,3] That infinitesimal vortices can be "smeared out" to finite-area vortex patches with constant vorticity to achieve equilibria has attracted interest due to its relevance to large-scale geophysical flows and coherent flow structures observed in quasi-geostrophic or two-dimensional turbulence. Arguably, the simplest non-trivial vortex patch equilibrium is the Kirchhoff vortex, a steady rotating solution of the 2D Euler equations. The Kirchhoff vortex is an elliptical patch of constant vorticity with axis lengths a and b, surrounded by fluid having zero vorticity,[4] i.e., a monopolar equilibrium. Linear[5] and non-linear[6] stability analyses conclude that for aspect ratios such that $1/3 < b/a < 3$, the Kirchhoff vortex is stable. Other examples include monopolar rotating equilibria with m-fold symmetry, named V-states,[7] and steady translating dipoles[8] (equal and opposite-signed vortex patches), both of which have been computed numerically using contour dynamics.[9] For given N-fold symmetry, rotating V-states are uniquely defined by two characteristic radii R_1 and R_{M+1}, as shown in Fig. 1(a), and there exists a limiting ratio of two characteristic radii R_1/R_{M+1} beyond which no equilibria can be found. A local expansion of the streamfunction[10,11] leads to the conclusion that these limiting states must have a non-continuous tangent with 90° jumps (corners) or 180° jumps (cusps) on the patch boundary. Monopolar V-states have been shown to have limiting states with corners. In addition to these, there exist special exact solutions with cusp-like limiting states characterised by zero velocity on the boundary.[12,13] These solutions exist in the presence of a

[a]Electronic mail: bin.xue.09@ucl.ac.uk
[b]Electronic mail: e.johnson@ucl.ac.uk
[c]Electronic mail: n.r.mcdonald@ucl.ac.uk

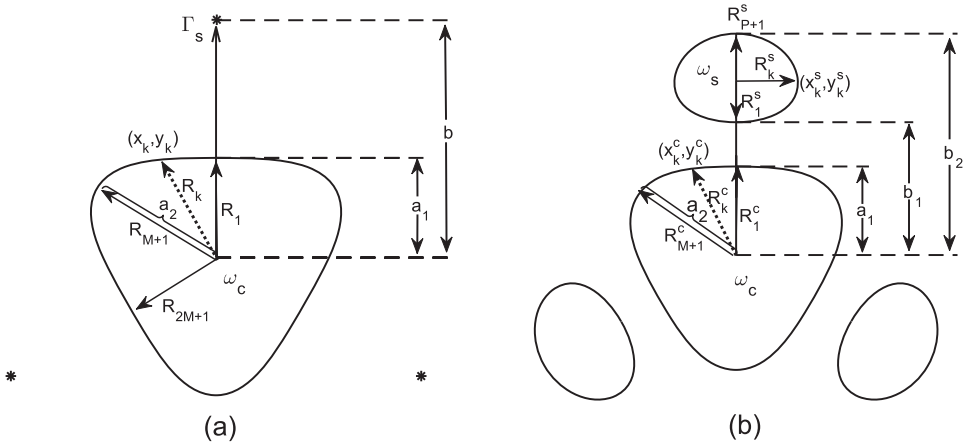

FIG. 1. Schematic diagram of (a) "3 + 1" point vortex-vortex patch equilibria with the point vortex locations indicated by the dots and (b) "3 + 1" multipolar vortex equilibria along with their boundary point discretizations and parameters for numerical considerations.

background straining field or when there are surrounding point vortices.

Other numerically computed vortex equilibria include co-rotating vortex pairs[14] and N patches arranged on the corners of a rotating N-polygon.[15,16] More recently, numerical and laboratory experiments[17–26] indicate the existence of coherent rotating tripolar vortex structures, and higher connectivity analogs have also been found numerically.[27,28] Further analytical studies of the vortex equilibrium problem can be found in other studies.[25,29–31] Numerical studies and laboratory simulations[21,28,32–34] indicate that these multipolar vortex equilibria with zero total circulation can be generated through barotropic instability of a shielded vortex, i.e., a circular vortex with zero total circulation. The multipolar vortex equilibria of zero total circulation have a central patch of vorticity surrounded by N opposite-signed identical satellite vortex patches. These equilibria including those having a same-signed vorticity central patch found here belong to a more general class which here will be called "N + 1" multipolar vortex equilibria, where "1" refers to the single central patch at the origin. The linear stability[35] of "N + 1" point vortex equilibria depends on the ratio of the circulation of the central point vortex to the circulation of a satellite point vortex. Such equilibria are linearly stable for a range of circulation ratios, both negative and positive. The additional presence of a same-signed central point vortex has been shown to make the N-polygon point vortex structures more stable.[35] Apart from these 2D vortex equilibria, geophysical tripolar vortex equilibria in a two-layer fluid have been found numerically and studied recently.[36–38]

A further, new, class of multipolar vortex equilibria are computed here: finite-area vortex equilibria consisting of two sets of nested polygonally arranged vortex patches, i.e., a structure comprising two sets of identical vortex patches arranged at the vertices of polygons of different sizes but sharing the same centre. There exist two distinct cases: when the two sets of polygonal patches are aligned with each other and when they are staggered. Each case has two distinct families of solutions corresponding to the polygonally arranged patches having the same-signed vorticity or opposite-signed vorticity.

Section II gives the dynamical background and details of the numerical routine based on second-order contour dynamics[7] for computing "N + 1" point vortex-vortex patch equilibria. The limiting solutions are discussed, and a linear stability analysis is presented. Section III computes "N + 1" multipolar vortex equilibria, and various limiting state behaviours are investigated. These equilibria are simulated in a time-dependent integration in order to test their stability. In Sec. IV, new finite-area equilibria are found numerically, which are called here the "N + N" equilibria. Results are compared and connections are made to the existing equilibria. Finally, Sec. V gives a summary and discussion.

II. BACKGROUND

A vortex patch is a finite region of fluid in which the vorticity is constant. The velocity field (u, v) at (x, y) induced by a set of vortex patches enclosed by boundaries ∂D_i with vorticity ω_i can be written as[7]

$$(u,v)(x,y) = -\sum_{i=1}^{\widetilde{N}} \frac{\omega_i}{2\pi} \int_{\partial \mathrm{D}_i} \left[(x - X_i', y - Y_i')/l'\right] \mathrm{d}l', \quad (1)$$

where $\widetilde{N}$ is the number of vortex patches, $(X_i', Y_i') \in \partial D_i$, and $l'(x, X', y, Y') = \sqrt{(x - X')^2 + (y - Y')^2}$. For a steady rotating vortex, the velocity $\mathbf{u} = (u, v)$ on the vortex boundary satisfies

$$(\mathbf{u} - \mathbf{\Omega} \wedge \mathbf{x}) \cdot \mathbf{n} = 0, \quad (2)$$

where $\mathbf{\Omega} = \Omega\mathbf{k}$, $\mathbf{k}$ is a unit vector orthogonal to the plane of the patch, and Ω is the angular speed of the equilibria. The boundaries of vortex patches in a time-dependent simulation evolve according to

$$\left(\frac{\mathrm{d}X_i}{t}, \frac{\mathrm{d}Y_i}{t}\right) = (u,v)|_{x=X_i, y=Y_i}. \quad (3)$$

It is assumed that all the equilibria computed here are in steady rotation with some angular speed Ω, which is to be found. All numerical routines used here are modified forms of the iterative routines developed by Wu, Overman, and Zabusky[7] (hereafter WOZ, see Appendix A) and are based on a contour dynamics routine to compute the velocities on patch boundaries.

A. "N + 1" point vortex–vortex patch equilibria

Consider equilibria in which a central, finite area, vortex patch with vorticity ω_c is surrounded by N identical point vortices of strength Γ_s [see Fig. 1(a)]. Hereafter this equilibrium

type is called a "$N + 1$" point vortex-vortex patch equilibrium. Requiring the central patch to have N-fold symmetry reduces the number of parameters for these states to 5: two characteristic radii of the central patch R_1 and R_{M+1}, the radial distance b of the point vortices to the origin, ω_c (or the total circulation of the patch Γ_c), and Γ_s, the circulation of the satellite point vortices. Prescribing four of them uniquely determines an equilibrium. Two modified WOZ methods have been used for computing the equilibria and are briefly described in Appendix B. One routine seeks convergent solutions with prescribed $R_1 = a_1$, b, ω_c, Γ_s, and the other prescribes $R_1 = a_1$, $R_{M+1} = a_2$, b, ω_c. The two methods give matching results. Fixing the two characteristic radii R_1 and R_{M+1} of the central patch while relaxing the constraint on Γ_s reveals a family of solutions with a limiting state central patch. Figure 2 shows families of equilibria obtained by prescribing R_1 and R_{M+1} with values a_1 and a_2 for various ratios a_2/a_1. The solutions are normalised so that the satellite point vortices have unit strength and are unit distance from the origin, i.e., $\Gamma_s = 1$ and $b = 1$. The circulation ratio of the central patch to point vortex is denoted $\alpha = \Gamma_c/\Gamma_s$. There are two distinct families of solutions: the equilibria with $a_2/a_1 > 1$ have corresponding $\alpha < 0$ (i.e., central patch and satellite patches have opposite-signed circulation), while those with $a_2/a_1 < 1$ have corresponding $\alpha > 0$ (same-signed circulation). For opposite-signed equilibria, the boundary of the central patch flattens on the side nearest to the surrounding point vortices as shown in Figs. 2(a)–2(c), while for same-signed ($\alpha > 0$) equilibria, the boundary of the central patch elongates towards each of the surrounding point vortices as shown in Figs. 2(d)–2(f).

Solution families are computed and limiting states are approached by increasing or decreasing the a_2/a_1 ratio. The limiting states of the $\alpha > 0$ family acquire corners on the central patch boundary when a_2/a_1 is decreased to a minimum as shown in Figs. 2(d)–2(f). Limiting states of the $\alpha < 0$ family are approached when a_2/a_1 is increased to a maximum as shown in Fig. 3. As the limiting states are approached, stagnation points of the flow (not shown), found on the lines of symmetry of the central patch, move towards the patch. Thus in Figs. 2(d)–2(f), the limiting states have stagnation points on the corners for $\alpha > 0$ equilibria, while the limiting states for $\alpha < 0$ equilibria, as shown in Fig. 3, have stagnation points at the tips of the central patch.

To illustrate the complete solution for the families with a given choice of a_1, the inverse circulation ratio $1/\alpha$ is plotted against a_2/a_1 in Fig. 4. The inverse circulation ratio changes sign when the aspect ratio $a_2/a_1 = 1$, i.e., a circular patch, and the satellite vortices have zero strength. Note also that increasing the number of satellite point vortices gives a shorter range of solutions for a_2/a_1 but supports a larger central patch. It is expected that when $N \to \infty$, the equilibrium must have a circular central patch. As $a_1 \to 0$, i.e., a smaller central

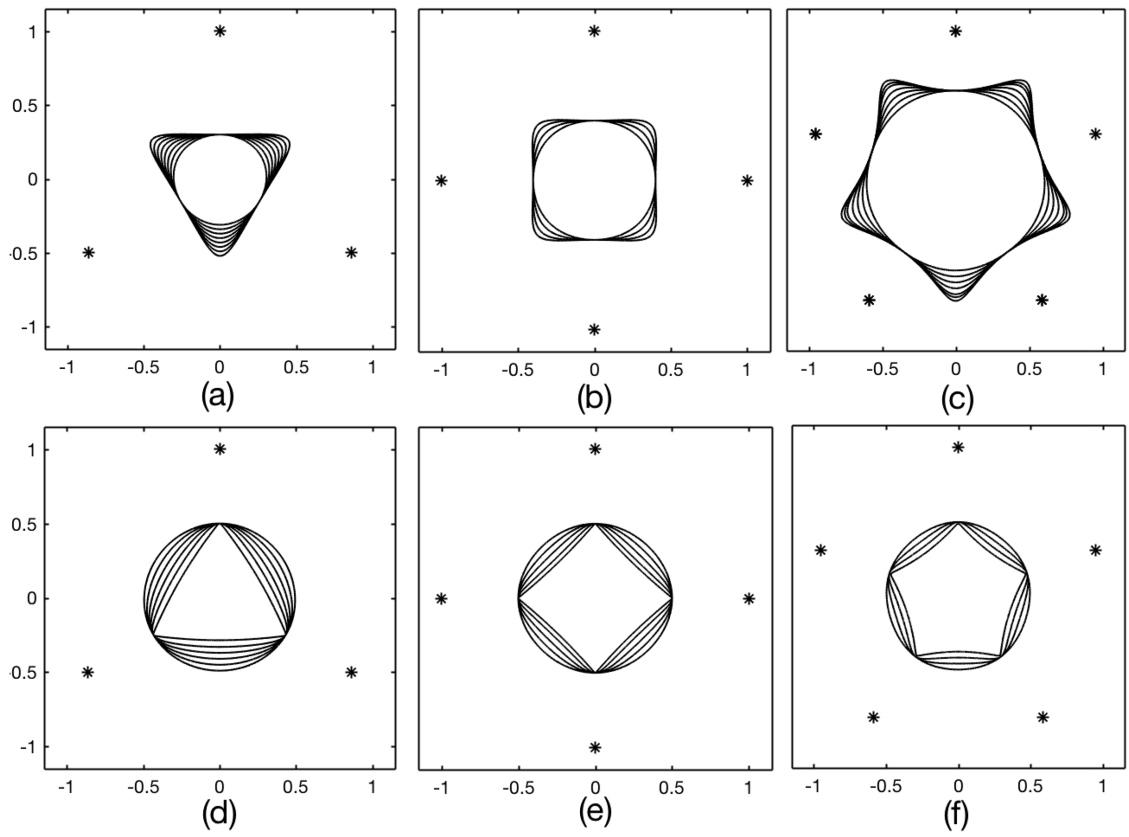

FIG. 2. Families of solutions of normalised (i.e., $b = 1$ and $\Gamma_s = 1$) "$N + 1$" point vortex-vortex patch equilibria with 3-, 4-, and 5-fold symmetry. The point vortices are indicated by the stars. (a)–(c) show opposite-signed equilibria ($\alpha < 0$) with solutions corresponding to (a) $a_1 = 0.3$ with values of a_2 from a_1 increasing to 0.541, (b) $a_1 = 0.4$ with values of a_2 from a_1 increasing to 0.524, and (c) $a_1 = 0.6$ with values of a_2 from a_1 increasing to 0.814. (d)–(f) show same-signed equilibria ($\alpha > 0$) with solutions corresponding to (d) $a_1 = 0.5$ with values of a_2 from a_1 decreasing to 0.285, (e) $a_1 = 0.5$ with values of a_2 from a_1 decreasing to 0.34, and (f) $a_1 = 0.5$ with values of a_2 from a_1 decreasing to 0.375.

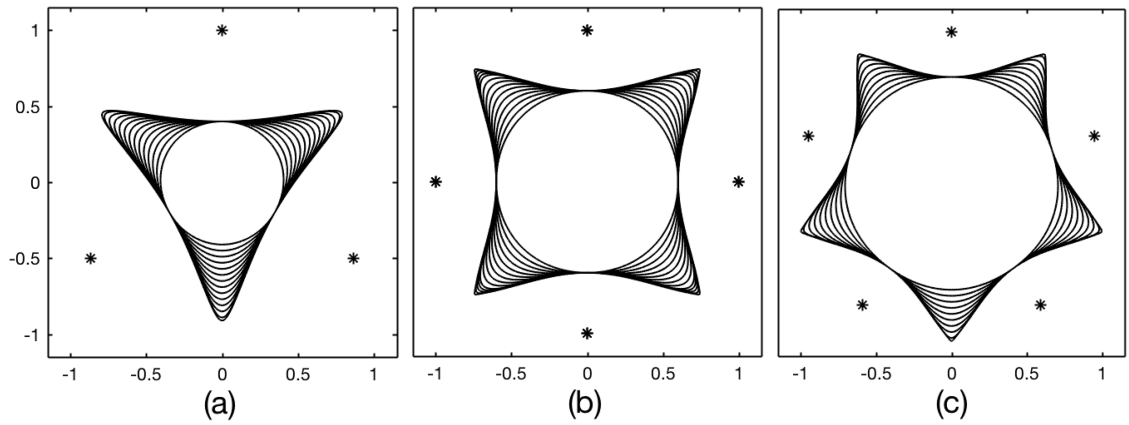

FIG. 3. Equilibrium families of normalised opposite-signed "$N + 1$" point vortex-vortex patch equilibria with 3-, 4-, and 5-fold symmetry. Solutions correspond to (a) "3 + 1" equilibria having $a_1 = 0.4$ with values of a_2 from a_1 up to 0.94, (b) "4 + 1" equilibria having $a_1 = 0.6$ with values of a_2 from a_1 up to 1.05, and (c) "5 + 1" equilibria having $a_1 = 0.7$ with values of a_2 from a_1 up to 1.05.

patch, equilibria with an infinite range of circulation ratios $-\infty \leq \alpha \leq \infty$ are recovered as in the "$N + 1$" point vortex equilibria.[35]

B. Discussion of limiting states of normalised solutions

A local expansion of the streamfunction method[10] leads to the conclusion that limiting state m-fold rotating vortex equilibria have jumps in a tangent slope of 90° (corners) on their boundary, although it does not rule out the possibility of a cusp-type limiting state in other scenarios involving the presence of background flows, possibly due to other vortices. As found here, limiting corner-like equilibria arise in same-signed solution families, and limiting states with a tip-like central patch arise in the opposite-signed solution families. For opposite-signed equilibria, there exist analytical results with limiting states[12,13] having cusps, these being the equivalent of the tips of the normalised solutions presented here. These solutions either have surrounding point vortices on the "flat" side of the central patch[13] as in the numerical solutions presented here or involve a patch embedded in a straining field that provides an equivalent effect.[12] They both share the property that the tangential and normal velocities on the patch boundary are identically zero when viewed in the rotating frame, and

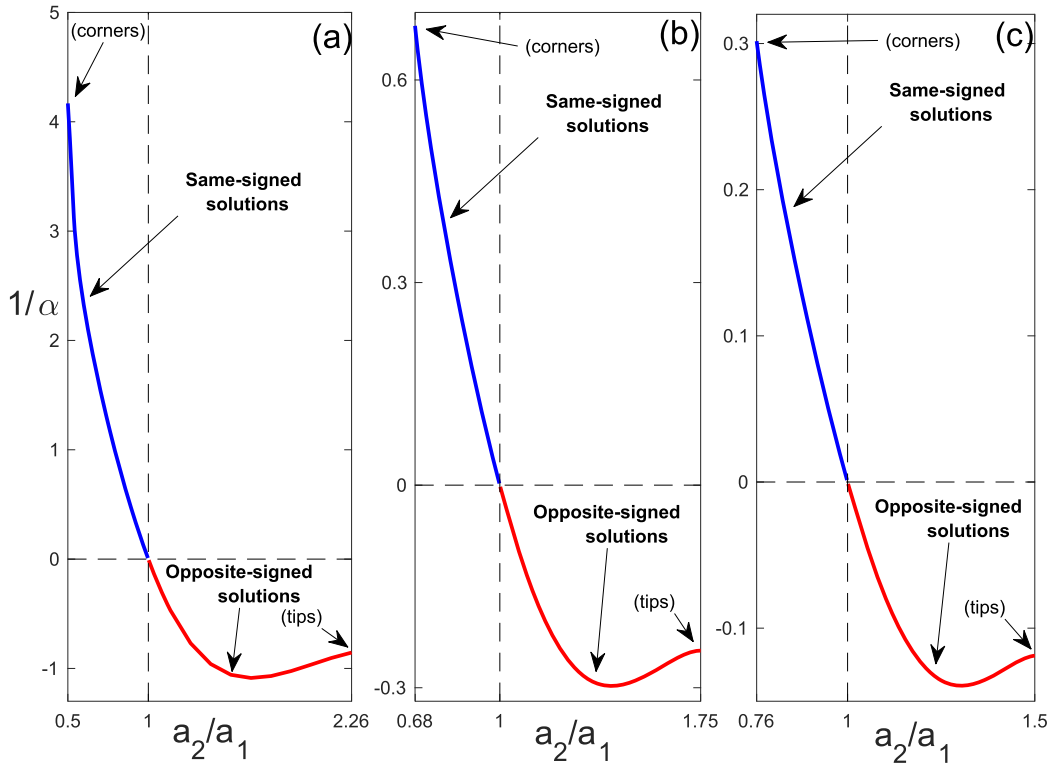

FIG. 4. Plots of inverse circulation ratio $1/\alpha$ against a_2/a_1 for complete families of solutions with 3-, 4-, and 5-fold symmetry. (a) "3 + 1" solutions with $a_1 = 0.4$. (b) "4 + 1" solutions with $a_1 = 0.6$. (c) "5 + 1" solutions with $a_1 = 0.7$. Minimum a_2/a_1 corresponds to same-signed limiting equilibria with corners, and the maximum a_2/a_1 corresponds to opposite-signed limiting equilibria with tips.

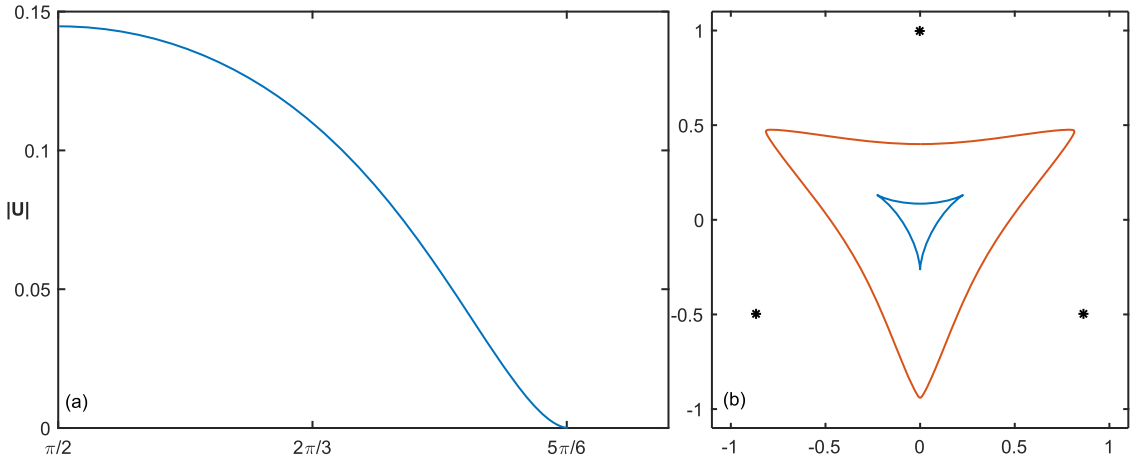

FIG. 5. Comparisons of numerically computed limiting state opposite-signed "3 + 1" equilibrium and the exact limiting state solution.[13] (a) The absolute velocity profile on the $1/(2N)$ section of the central patch boundary of the numerically produced equilibrium in a rotating frame. (b) Outer central patch corresponds to numerically produced limiting state for prescribed $a_1 = 0.4$ and $a_2 = 0.94$ giving $\alpha = -1.19$, and inner central patch corresponds to Crowdy's[13] exact solution having cusps with parameters $a_1 = 0.085$, $a_2 = 0.261$, and $\alpha = -0.0149$.

the equilibria have a steady rotational speed of exactly $\omega_c/2$. Crowdy's exact solutions with surrounding point vortices[13] lie outside the range of solutions that are capable of being computed by the numerical routine used here. In Fig. 5(a), the absolute velocity in the rotating frame for a numerically computed "3 + 1" limiting state opposite-signed equilibrium is plotted against θ for the section of central patch boundary points defined by R_1 to R_{M+1} as in Fig. 1(a), where θ is the angle of patch boundary points relative to the origin. The patch boundary attains the maximum absolute velocity at R_1 and gradually decreases towards zero at the tips as shown in Fig. 5(a). By contrast, the exact analytical solution[13] has zero velocity profile for all θ. Figure 5(b) plots the numerically produced opposite-signed "3 + 1" limiting state solution and Crowdy's[13] exact, analytical, cusped solution scaled so the point vortices coincide. This shows the exact analytical solution to be a special solution of the opposite-signed family of solutions, which could not be obtained by the numerical method here due to the appearance of arbitrarily high curvature as the vortex tips become more cusplike.

C. Linear stability analysis

The linear stability of both N-polygon point vortex equilibria (N identical point vortices arrange at the vertices of N-polygon) and the analogous finite-area N-polygon co-rotating vortex patch equilibria (i.e., with the surrounding point vortices replaced by patches whose shape is numerically computed) have been thoroughly studied.[39] N-polygon point vortex equilibria are linearly stable if $N \leq 7$ and unstable for $N \geq 8$. This mode of instability for $N \geq 8$ will be referred to as "circular" instability since it is manifested by a breach of the point vortices initially arranged on a circle about the centre of rotation. If a central vortex is added, then linear stability analysis of "N + 1" point vortex equilibria[35] with the satellite point vortices with unit distance from the central patch reveals stability regions within which the configurations are Lyapunov stable. There are two instability mechanisms:[35] (i) central point vortex instability, where the location of the central point vortex is unstable if α is below the lower negative threshold, and (ii) circular instability affecting the surrounding N point vortices if α is above the upper positive threshold. The presence of the same-signed central point vortex is shown to stabilize the N-polygon point vortex equilibria.[35]

To study the effect of a finite-area central patch in the "N + 1" equilibria, consider a perturbation on the central patch boundary while keeping the point vortices fixed. Consider a perturbed central patch boundary

$$r(\theta) = r_0(\theta) + \hat{r}(\theta)e^{\sigma t}, \tag{4}$$

where r_0 is the unperturbed central patch boundary in an "N + 1" equilibrium and the second term is the small perturbation ($\hat{r} \ll r_0$) to the boundary which is in the form of a normal mode. The real part of σ is the growth rate, and the imaginary part is the frequency of the boundary disturbance. The form of $\hat{r}(\theta)$ is expressed as

$$\hat{r}(\theta) = r_0(\theta) \sum_{i=1}^{M} C_i \phi_i(\theta), \tag{5}$$

where ϕ_i are the orthonormal functions

$$\pi^{\frac{1}{2}}\phi = \left(\frac{1}{\sqrt{2}}, \cos\theta, \ldots, \cos P\theta, \sin\theta, \ldots, \sin P\theta\right). \tag{6}$$

Hence $M = 2P + 1$ and C_i are the coefficients to be determined. The points on the perturbed boundary move with local fluid velocity

$$\frac{\partial r}{\partial t} + \frac{u_\theta}{r}\frac{\partial r}{\partial \theta} = u_r, \tag{7}$$

where u_θ and u_r are the tangential and radial velocities on the patch boundary in the rotating frame with the contributions of fixed point satellite vortices taken into account. Now substitute (4) into (7) and define the first order deviation

$$\epsilon(\theta) = \sigma\hat{r} - \frac{u_{\theta 0}}{r_0^2}\frac{dr_0}{d\theta}\hat{r} + \frac{u_{\theta 0}}{r_0}\frac{d\hat{r}}{d\theta} + \frac{1}{r_0}\frac{dr_0}{d\theta}\hat{u}_\theta - \hat{u}_r, \tag{8}$$

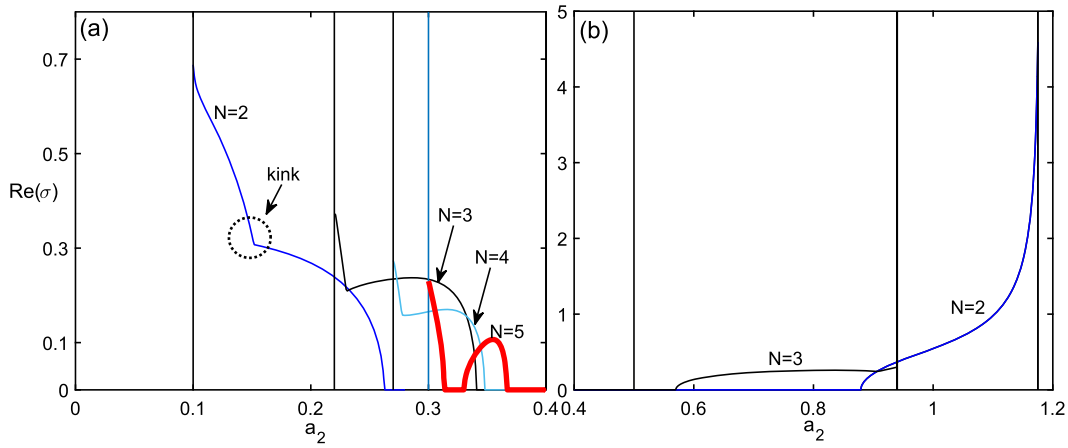

FIG. 6. Max over i, $i = 1, 2, \ldots, M$ the absolute real part of eigenvalues Re($|\sigma|$) plotted against values of a_2 for a family of equilibria with $a_1 = 0.4$ fixed. (a) Same-signed equilibria with $a_2 < a_1$. The thick line is for the $N = 5$ case. (b) Opposite-signed equilibria with $a_2 > a_1$. The vertical lines indicate the lower and upper limits of a_2 beyond which no equilibria are found.

where $u_{\theta 0}$ is the unperturbed tangential velocity and $\hat{u}_\theta$ and $\hat{u}_r$ are the perturbation velocities. Then apply the Galerkin method by requiring that

$$\int_0^{2\pi} \epsilon(\theta')\phi_i(\theta')d\theta' = 0, \quad i = 1, 2, \ldots, M. \tag{9}$$

This leads to an eigenvalue problem

$$\sigma \boldsymbol{C} = \boldsymbol{A}\boldsymbol{C}, \tag{10}$$

where $\boldsymbol{C} = (C_1, C_2, \ldots, C_M)$ and $\boldsymbol{A}$ is a real $M \times M$ matrix. In the computation here, $M = 201$ and Eq. (10) can be used to find the complex eigenvalues σ_i, $i = 1, 2, \ldots, M$. The maximum growth rate, max($\mathbf{Re}(\sigma_i)$), $i = 1, 2, \ldots, M$, is plotted against values of a_2 in Fig. 6 for normalised solutions of "$N + 1$" point vortex-vortex patch equilibria with fixed $a_1 = 0.4$. Figure 6(a) shows the maximum growth rate for same-signed equilibria, and Fig. 6(b) shows the maximum growth rate for opposite-signed equilibria. Recall also that $a_2 < a_1$ corresponds to same-signed equilibria, and $a_2 > a_1$ corresponds to opposite-signed equilibria.

When $|a_2 - a_1|$ is small, the central patch is near circular, the absolute relative circulation ratio $|\alpha|$ is large, and the central patch is linearly stable. On the other hand, when $a_2 - a_1$ approaches the upper and lower limits so that the central patch is relatively weak ($|\alpha|$ small) and has distinct non-circular boundary developing corners or tips as shown in Figs. 2 and 3, the central patch is linearly unstable. The kinks in the growth rate of the instability of the same-signed solution region in Fig. 6(a) indicate the transition from circular to central patch instability. This is especially evident for case $N = 5$ (i.e., "5 + 1" equilibria) shown by the thick line where a small linear stable region lies between two separate linearly unstable regions. The different modes of instability are illustrated later when discussing the time-dependent evolution. The opposite-signed equilibria have only one linear instability region, which indicates that these are more stable than their same-signed counterparts. Figures 6(a) and 6(b) also reveal that same-signed equilibria have generally smaller linearly stable regions than opposite-signed equilibria. Increasing the number of satellite point vortices makes the central patch more stable for both same and opposite-signed equilibria. Increasing the number of satellite point vortices eventually introduces the circular instability with the polygonally arranged satellite vortices becoming unstable.[35]

III. MULTIPOLAR VORTEX EQUILIBRIA

Now consider the "$N + 1$" multipolar vortex equilibria in which a central patch is surrounded by N identical satellite patches [see Fig. 1(b)]. That is, the point vortices are replaced by patches. This configuration has one degree of freedom more than the "$N + 1$" point vortex-vortex patch equilibria: two characteristic radii R_1^c, R_{M+1}^c for the central patch, two boundary points corresponding to R_1^s, R_{P+1}^s for the satellite patches, and their respective vorticities ω_c and ω_s (or their circulations Γ_c, Γ_s). Here superscripts and subscripts, c, s, refer to variables for the central patch and satellite patches. Symmetry considerations dictate that the central patch has an N-fold symmetry and the satellite patches have a mirror symmetry [see Fig. 1(b)], so only discretized points on fundamental sectors of the vortex patch boundaries need be considered in the numerical computation. Let $M + 1$ be the number of points on a $1/2N$ section of the central patch and $P + 1$ be the number of points on one half of the symmetric boundary of a satellite patch. These boundaries are discretized relative to the "centre" of individual patches with evenly spaced θ as in Appendix A.

As in the case of the "$N + 1$" point vortex-vortex patch equilibria, there exist two distinct families of solutions: one with a central patch having opposite-signed vorticity to the satellite patches and the other with all patches having the same-signed vorticity. Previous results[27,28] exist for opposite-signed multipolar vortex equilibria for the special case of zero total circulation. The same-signed multipolar vortex equilibria obtained here are new, so are the opposite-signed equilibria with non-zero total circulation. Together they give a complete class of "$N + 1$" multipolar vortex equilibria. Different modified WOZ methods have been used here for

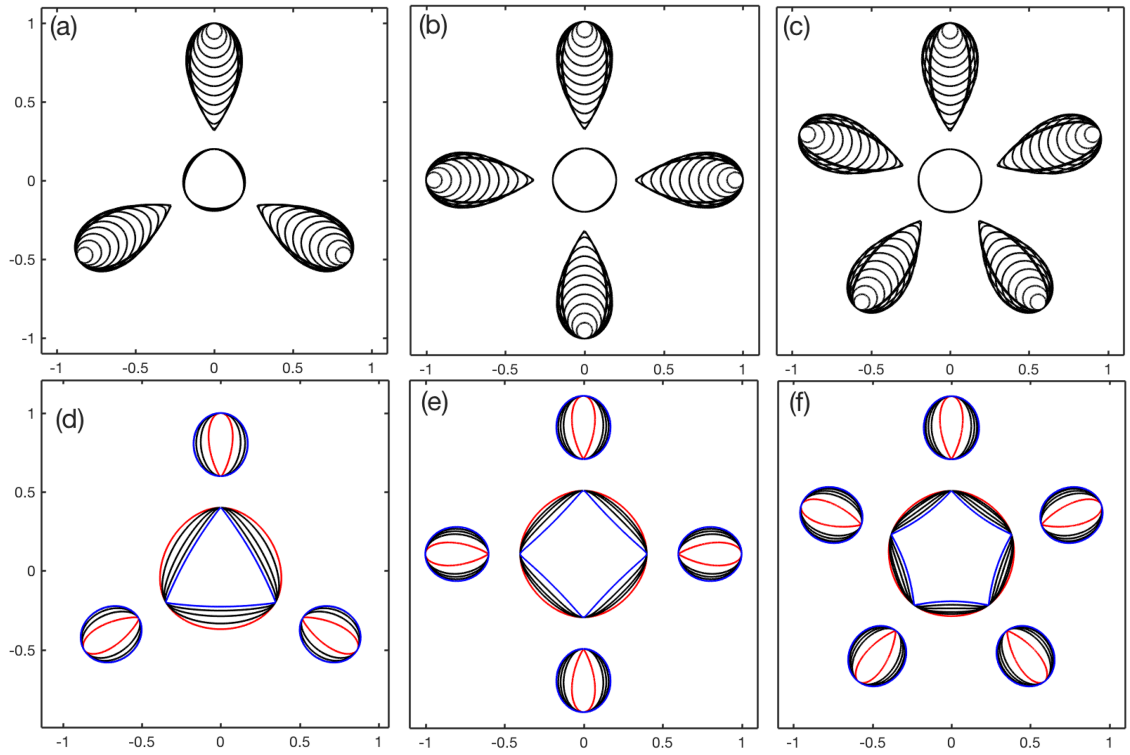

FIG. 7. Families of solutions of same-signed multipolar vortex equilibria with 3-, 4-, and 5-fold symmetry. For (a)–(c), the families have $a_1 = 0.2$, $b_2 = 1$, and $\omega_c = \omega_s = 1$ with decreasing values of b_1 from 0.9 so that satellite patches increase in size towards limiting states. (a) Limiting value $b_1 = 0.316$. (b) Limiting value $b_1 = 0.32$. (c) Limiting value $b_1 = 0.314$. For (d)–(f), the families have $a_1 = 0.4$, $b_1 = 0.6$, $b_2 = 1$, $\omega_c = 1$ with decreasing values of α corresponding to a weaker central patch and a boundary tending to limiting states with corners. (d) α from 7 to a limiting value of 0.75. (e) α from 7.5 to a limiting value of 0.8. (f) α from 7.5 to a limiting value of 0.8.

computations: one approach prescribes a_1, b_1, b_2, ω_c, and ω_s following other authors;[27,28] another prescribes a_1, a_2, b_2, ω_c, ω_s (or the circulations Γ_c and Γ_s in place of their strengths). The latter approach prescribes two characteristic radii of the central patch while relaxing the constraint on the inner boundary point b_1 of the satellite patches. A further approach employed here prescribes a_1, a_2, b_1, b_2, and ω_c (or α, the circulation ratio) and has proved effective in finding new finite-area vortex equilibria. Details are given in Appendix C. These different methods have been cross-checked and found to agree with each other.

A. Numerical results and discussions

The numerical solutions reveal two limiting behaviours for each family of "N + 1" multipolar vortex equilibria, dependent on the relative vorticity strengths of the central patch to the satellite patches. One way to illustrate the limiting behaviours is by prescribing the same characteristic radii a_1, b_1, and b_2 with various circulation ratios of patches as shown in Figs. 7(d)–7(f) for same-signed "N + 1" multipolar vortex equilibria. In this case, the two limiting states are evident by decreasing the circulation ratio α. When α is large and at

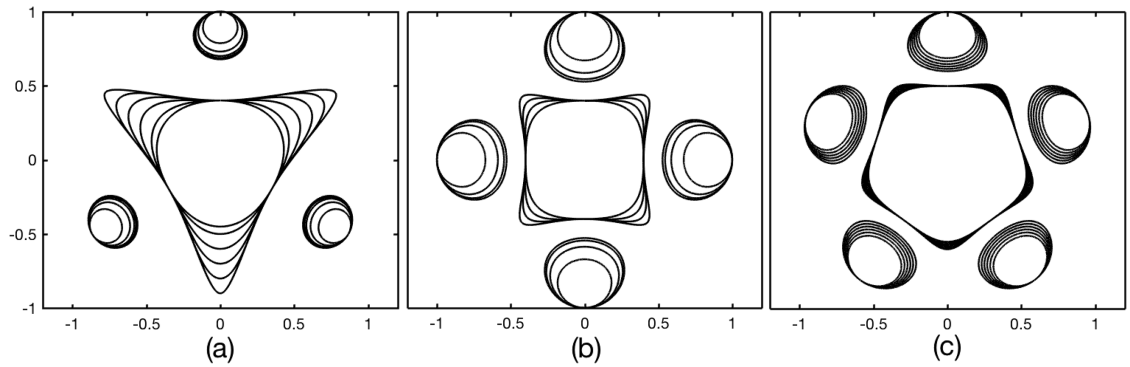

FIG. 8. Opposite-signed multipolar equilibria computed by prescribing a_1, a_2, b_2, ω_c, and ω_s defined in Fig. 1(b); family of solutions corresponds to various values of a_2 with other parameters fixed. (a) "3 + 1" equilibria with $a_1 = 0.4$, $a_2 = 0.9, 0.8, 0.7, 0.6, 0.5, 0.45$, $b_2 = 1$, $\omega_c = 1$, $\omega_s = -4$. (b) "4 + 1" equilibria with $a_1 = 0.4$, $a_2 = 0.6, 0.55, 0.5, 0.45$, $b_2 = 1$, $\omega_c = 1$, $\omega_s = -4$. (c) "5 + 1" equilibria with $a_1 = 0.5$, $a_2 = 0.6, 0.59, 0.58, 0.57, 0.56, 0.55$, $b_2 = 1$, $\omega_c = 1$, $\omega_s = -3.5$.

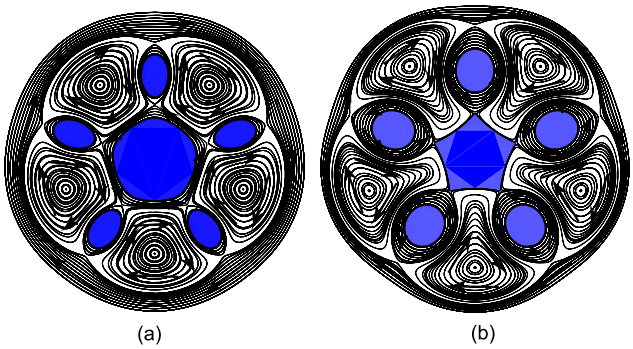

FIG. 9. Streamline plots of "5 + 1" same-signed multipolar equilibria with the shaded regions being the vortex patches having same-signed vorticity. Arrows are added to indicate the direction of flows. (a) $a_1 = 0.4$, $b_1 = 0.6$, $b_2 = 1$, $\omega_c = 1$, $\omega_s = 2$. (b) $a_1 = 0.4$, $b_1 = 0.6$, $b_2 = 1$, $\omega_c = 1$, $\omega_s = 3.922$.

its maximum, the central patch is relatively strong and so has a near-circular shape, while the satellite patches have oval shapes with tips close to the central patch. When α decreases towards a minimum, the central patch becomes relatively weak and eventually exhibits corners on its boundary, while the satellite patches are relatively strong and have near-elliptical shape. Another way to illustrate the limiting behaviour is by varying one characteristic radius: for example, Figs. 7(a)–7(c) give equilibria with increasing sizes of satellite patches by prescribing decreasing values of b_1. Similar limiting N-polygon co-rotating patches as in Figs. 7(a)–7(c) in the absence of the central patch have been computed by Dristchel.[15]

The opposite-signed "N + 1" equilibria are expected to have two limiting behaviours: one with the satellite patches approaching a limiting state that requires more sophisticated numerical treatment than the one used here and the other with the central patch approaching a limiting state. This is demonstrated in Fig. 8: for a sufficiently large central patch, the limiting state central patch acquires "tips" on its boundary. A common feature for opposite-signed equilibria is that the satellite patches flatten against the central patch as indicated in Fig. 8.

The streamline plots in Fig. 9 for two "5 + 1" same-signed multipolar vortex equilibria with different values of the vorticity ω_s in the satellite patches reveal different circulation regions. These streamlines are produced by advancing the fluid points outside the patches using the Runge-Kutta scheme. In both examples, there exist unstable stagnation points between the central patch and the satellite patches due to the opposing flows produced by them. When the central patch tends to its limiting state, these stagnation points meet the corners of the central patch; see Fig. 9(b). When the satellite patches tend to their limiting states, these stagnation points meet the tips of the satellite patches (not shown). Stable stagnation points are also evident in Fig. 9. New equilibria can, in principle, be computed by "growing" satellite patches of either positive or negative vorticity at such stable stagnation points. Indeed, the "N + 1" multipolar vortex equilibria themselves can be seen as the result of "growing" a central patch of either sign from existing "N"-polygonal co-rotating equilibria. New equilibria (not shown here) computed by placing point vortices at the stable stagnation points of "N + 1" multipolar vortex equilibria have also been obtained.

B. Fully non-linear evolutions

In this section, the time-dependent behaviour of the equilibria is investigated using contour surgery,[40] which allows vortex filamentation and merging. For all evolutions hereafter, the cutoff scale used in contour surgery is chosen to be $\mu = 0.1$, and the time step of the integrations is chosen to be $dt = 0.05$.

Consider "N + 1" multipolar vortex equilibria when the central patch is at, or near, its limiting state as in Fig. 10. Figure 10(a) shows the evolution of unstable opposite-signed "3 + 1" equilibria in which the tips eject filaments of vorticity that subsequently wrap around the satellite patches, and the

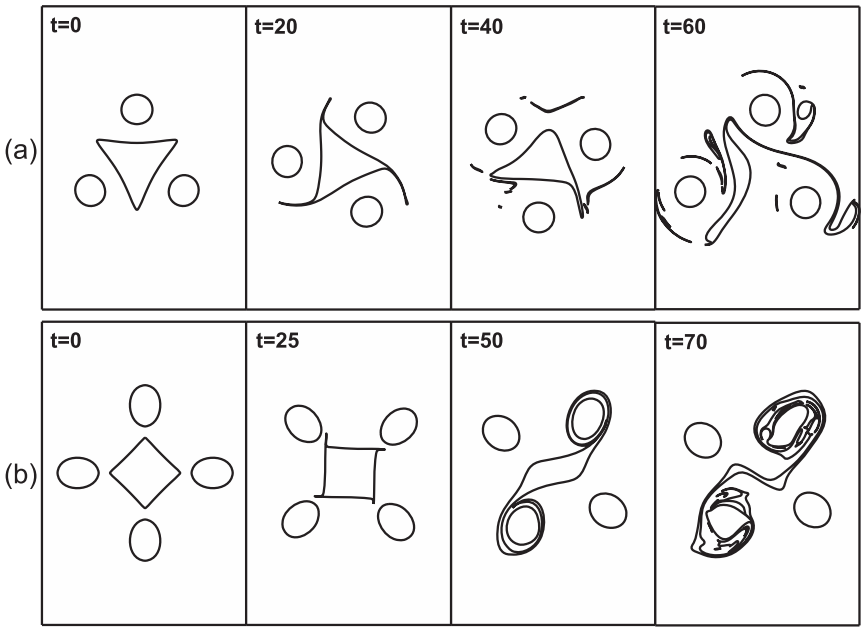

FIG. 10. (a) Evolution of the opposite-signed "3 + 1" equilibrium with $a_1 = 0.3$, $a_2 = 0.67$, $b_2 = 1$, $\omega_c = 1$, $\omega_s = -4$. (b) Evolution of the same-signed "4 + 1" equilibrium with prescribed $a_1 = 0.4$, $b_1 = 0.53$, $b_2 = 1$, $\omega_c = 1$, $\omega_s = 2.5$.

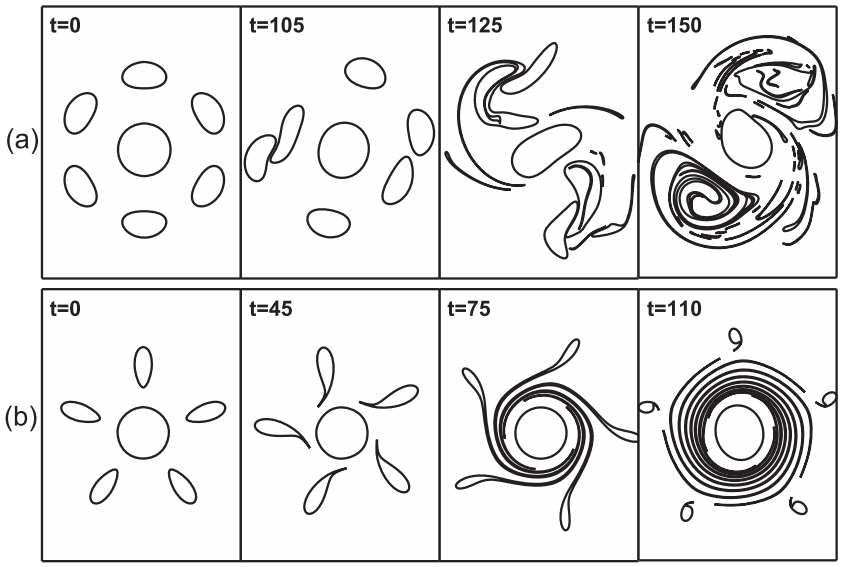

FIG. 11. (a) Evolution of the opposite-signed "6 + 1" equilibrium with $a_1 = 0.3$, $b_1 = 0.7$, $b_2 = 1$, $\omega_c = 2$, $\omega_s = -1$. (b) Evolution of the same-signed "5 + 1" equilibrium with $a_1 = 0.3$, $b_1 = 0.53$, $b_2 = 1$, $\omega_c = 1$, $\omega_s = 1.1$.

central patch eventually gets torn apart. This instability is a result of the flow field being strongest between the central patch and satellite patches: a small (linear) perturbation of the central patch boundary is expected to be swept towards the tips resulting in filamentation there. Unstable configurations for opposite-signed equilibria for the special case of zero total circulation have been thoroughly studied by Morel and Carton.[28]

Figure 10(b) shows the evolution of unstable same-signed "4 + 1" equilibrium in which the instability is manifested through the corners being drawn towards satellite patches. Again this is the result of the central patch having the largest velocity on its "flat" side and smallest at corners, an instability mechanism related to the linear stability result in Fig. 6(a) to the left of the "kinks." The right of the "kinks" in Fig. 6(a) arises from a different instability mechanism: it corresponds to equilibria with initially a less distorted central patch that is torn apart before any filamentation process.

The other limiting behaviour is when the central patch is relatively strong compared to the satellite patches ($|\alpha|$ large), i.e., the central patch is near circular. In the opposite-signed equilibrium, the satellite patches flatten against the central patch as shown in Fig. 11(a), while in the same-signed equilibrium, the satellite patches are tear-dropped with tips pointing towards the origin as shown in Fig. 11(b), which evolves into the final "2 + 1" state. The investigation of analogous "N + 1" point vortex equilibria[35] concludes that opposite-signed "N + 1" point vortex equilibria with a strong central vortex lead to the surrounding N-polygon satellite point vortices becoming unstable. This is evident for finite-area patches as in Fig. 11(a). For same-signed equilibria, the satellite patches are also unstable, undergoing filamentation from the tips of satellite patches as in Fig. 11(b). The shed filaments shield the central patch, while satellite patches remain in their equilibrium positions but are much reduced in area.

IV. NESTED POLYGONAL VORTEX EQUILIBRIA

An extension to steady rotating N-polygon point vortex equilibria, nested polygonal equilibria, has been found[2,3] consisting of N_1 identical point vortices of circulation Γ_1 centred at the vertices of a regular polygon whose vertices reside on a circle of radius R_1 and N_2 identical point vortices of circulation Γ_2 centred at the vertices of a regular polygon whose vertices reside on a circle of radius R_2. It has been shown[2,3] that for such equilibria to exist, N_1 must be equal to N_2

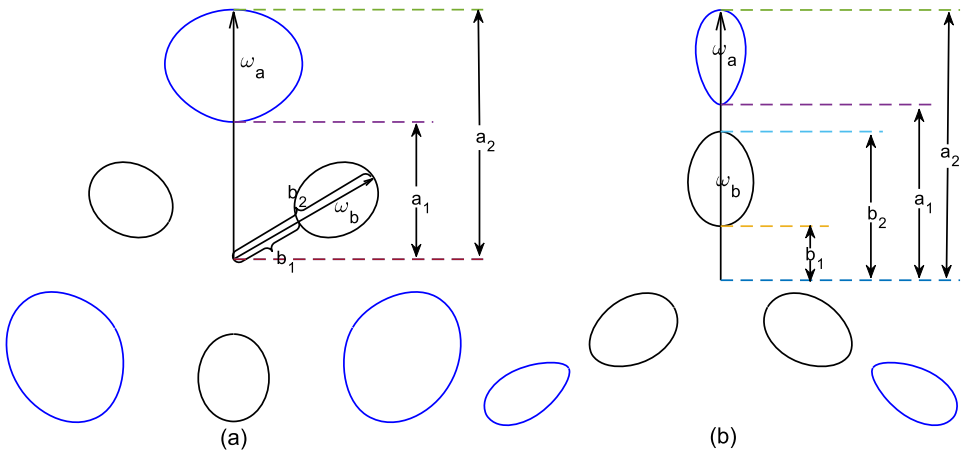

FIG. 12. Schematic diagram of "3 + 3" nested-polygons with the parameters that define an equilibrium. (a) Staggered, nested-polygons that are out-of-phase by an angle $\pi/3$. (b) Aligned, nested-polygons. The vorticities ω_a and ω_b can be either same-signed or opposite-signed.

(say $N_1 = N_2 = N$), and the vertices of the polygons can either be radially aligned with each other or out-of-phase (referred to here as "staggered") by an angle π/N. Figure 12 gives a schematic diagram of the analogous finite-area 3-fold symmetric nested-polygons that are uniquely defined by five of the parameters of characteristic radii a_1, a_2, b_1, b_2 and vorticities ω_a and ω_b (or, equivalently, their circulations Γ_a, Γ_b). Figure 12(a) gives a schematic diagram of staggered nested polygonal equilibria (hereafter, staggered "$N + N$" equilibria), and Fig. 12(b) gives a schematic diagram of polygonal equilibria in alignment (hereafter, aligned "$N + N$" equilibria), where N is the number of patches in each polygon. Note that all the vortex patches in consideration have mirror symmetry, so only discretized boundary points on half of the patch boundaries need to be considered in the computations. The numerical routine for obtaining equilibria by prescribing two characteristic radii for each set of identical patches (a_1, a_2, b_1, b_2 in this case) and strength of one set of patches, say ω_a, is given in Appendix C. For either aligned or staggered "$N + N$" equilibria, there again exist two distinct families of solutions: opposite-signed equilibria ($\alpha < 0$, where $\alpha = \Gamma_a/\Gamma_b$ is the total circulation ratio) and same-signed equilibria ($\alpha > 0$). The $N = 2$, 3 cases of different families of solutions are given below for illustration.

A. Aligned "*N* + *N*" equilibria

Families of solutions of same-signed aligned "$N + N$" equilibria are given in Fig. 13 for $N = 2$, 3. Two limiting behaviours are revealed by increasing the sizes of polygonal patches: Fig. 13(a) shows the limiting states with the outer set of patches tending towards tear shapes pointing towards the origin, and Fig. 13(b) shows the limiting state in which

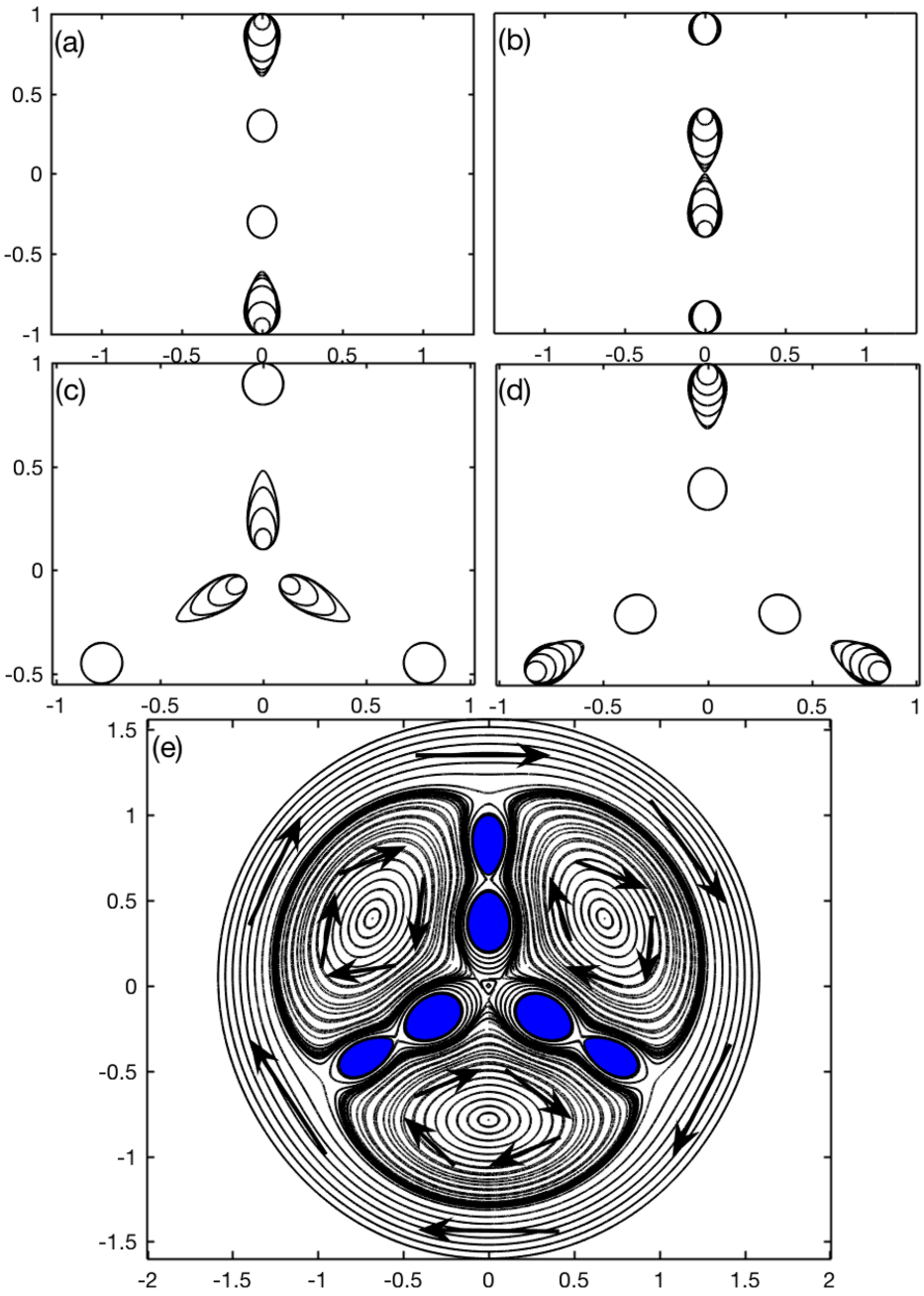

FIG. 13. Same-signed ($\alpha > 0$), aligned, "$N + N$" equilibria for $N = 2$, 3. (a) "2 + 2" equilibria with $a_1 = 0.9$, 0.8, 0.7, 0.65, 0.63, 0.61, $a_2 = 1$, $b_1 = 0.2$, $b_2 = 0.4$, $\omega_a = 1$ with $\omega_b = 0.268$, 1.24, 2.97, 3.79, 3.98, 4.05. (b) "2 + 2" equilibria with $a_1 = 0.8$, $a_2 = 1$, $b_1 = 0.3$, 0.2, 0.1, 0.05, 0.03, 0.01, 0.005, $b_2 = 0.4$, $\omega_a = 1$ with $\omega_b = 9.68$, 1.24, 0.37, 0.26, 0.23, 0.23, 0.23. (c) "3 + 3" equilibria with $a_1 = 0.8$, $a_2 = 1$, $b_1 = 0.1$, $b_2 = 0.2$, 0.3, 0.4, 0.48, $\omega_a = 1$ with $\omega_b = 0.22$, 0.15, 0.16, 0.18. (d) "3 + 3" equilibria with $a_1 = 0.9$, 0.85, 0.8, 0.75, 0.7, 0.68, $a_2 = 1$, $b_1 = 0.3$, $b_2 = 0.5$, $\omega_a = 1$ with $\omega_b = 0.27$, 0.68, 1.32, 2.15, 2.88, 2.96. (e) Streamlines for a "3 + 3" equilibrium with $a_1 = 0.65$, $a_2 = 1$, $b_1 = 0.2$, $b_2 = 0.55$, $\omega_a = 1$, $\omega_b = 1.16$. The shaded regions are the vortex patches having same-signed vorticity. Arrows indicate the direction of the flow field.

the inner set of patches touch at the origin. Figures 13(c) and 13(d) give the family of solutions for "3 + 3" equilibria, where Fig. 13(c) shows the limiting state where the inner set of patches become tear-shaped and point outwards towards the outer polygon patches. Figure 13(d) shows the limiting state with the outer set of patches pointing towards the origin. Figure 13(e) shows a streamline plot for a "3 + 3" equilibrium. There exist unstable stagnation points between the aligned patches, indicating existence of a possible instability mechanism.

In the opposite-signed case, only a limited range of solutions have been found for aligned equilibria (for $N = 2, 3$ cases) and none for $N \geq 4$. Figures 14(a) and 14(b) give examples of "2 + 2" and "3 + 3" equilibria for illustration. As expected, the opposite-signed patches flatten against each other. Figure 14(e) plots the streamlines for an opposite-signed aligned "3 + 3" equilibrium.

B. Staggered "*N* + *N*" equilibria

The family of solutions with same-signed, staggered "$N + N$" equilibria are given in Fig. 15 for $N = 2, 3$, in which limiting states are approached by increasing the sizes of one set of patches. The "2 + 2" equilibria exhibit different limiting states in comparison to "3 + 3" equilibria: Fig. 15(a) shows the limiting state "2 + 2" equilibria touching at the origin, while Fig. 15(b) shows the limiting state "3 + 3" having flattened shapes. These structures can be thought of as an extension to co-rotating vortex pairs and 3-polygon rotating structure by "growing" extra set of patches at the stable stagnation points viewed in the rotating frame. The idea of growing vortex patches at stagnation points to generate new, exact, equilibria has been used before by Crowdy and Marshall[41] to analytically construct special vortex equilibria. Streamlines in Fig. 15(e) give details of the flow field in the rotating frame for a "3 + 3" equilibrium.

The opposite-signed staggered "$N + N$" equilibria for $N = 2, 3$ cases have two distinct limiting behaviours as shown in Fig. 16. Scallop-like shapes for near limiting states of the outer set of patches are shown in Figs. 16(a) and 16(c). The limiting states of the inner set of patches in a "2 + 2" equilibrium touch at the origin as shown in Fig. 16(b), while "3 + 3" equilibria have long and thin inner patches as shown in Fig. 16(d). Streamlines in Fig. 16(e) give details of the flow field in the rotating frame for a "3 + 3" equilibrium.

C. Non-linear evolutions

Stability of the nested polygonal equilibria is explored using time-dependent simulation for the following scenarios: when either set of polygonal patches are at, or near, their limiting states and when the two sets of patches are "comparable" in sizes and strengths in the sense that they have boundary shapes not too different from circular or elliptical. A summary of the general findings is as follows:

1. The nested polygonal equilibria are generally less stable than the analogous "$N + 1$" multipolar vortex equilibria. Indeed, in some time-dependent simulations, they have been observed to evolve toward their multipolar equilibria counterparts.
2. The "2 + 2" equilibria are particularly unstable for both aligned and staggered nested polygonal equilibria, whereas "3 + 3" are the most stable equilibria.

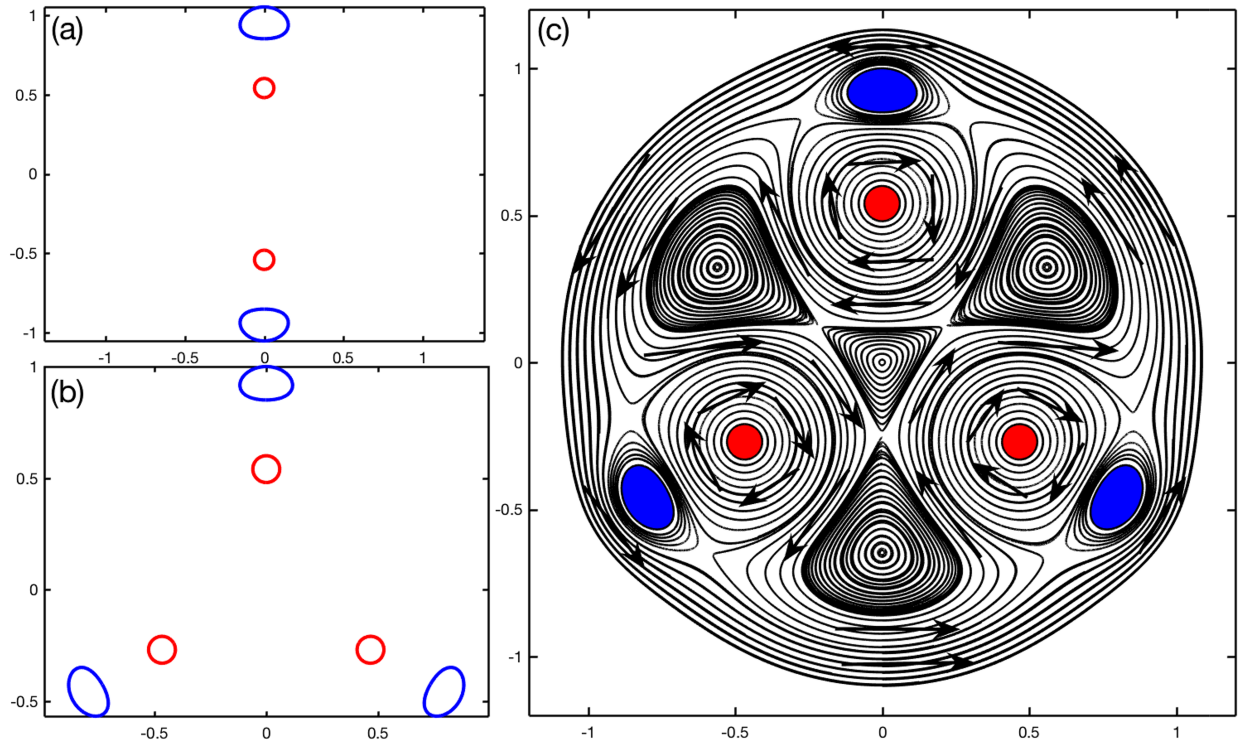

FIG. 14. Opposite-signed ($\alpha < 0$), aligned, "$N + N$" equilibria. (a) "2 + 2" equilibrium with $a_1 = 0.85$, $a_2 = 1.05$, $b_1 = 0.48$, $b_2 = 0.6$, $\omega_a = 1$, $\omega_b = -10.29$. (b) "3 + 3" equilibrium with $a_1 = 0.85$, $a_2 = 1$, $b_1 = 0.48$, $b_2 = 0.6$, $\omega_a = 1$, $\omega_b = -9.72$. (c) Streamlines for the "3 + 3" equilibrium in (b) with shaded regions being the vortex patches.

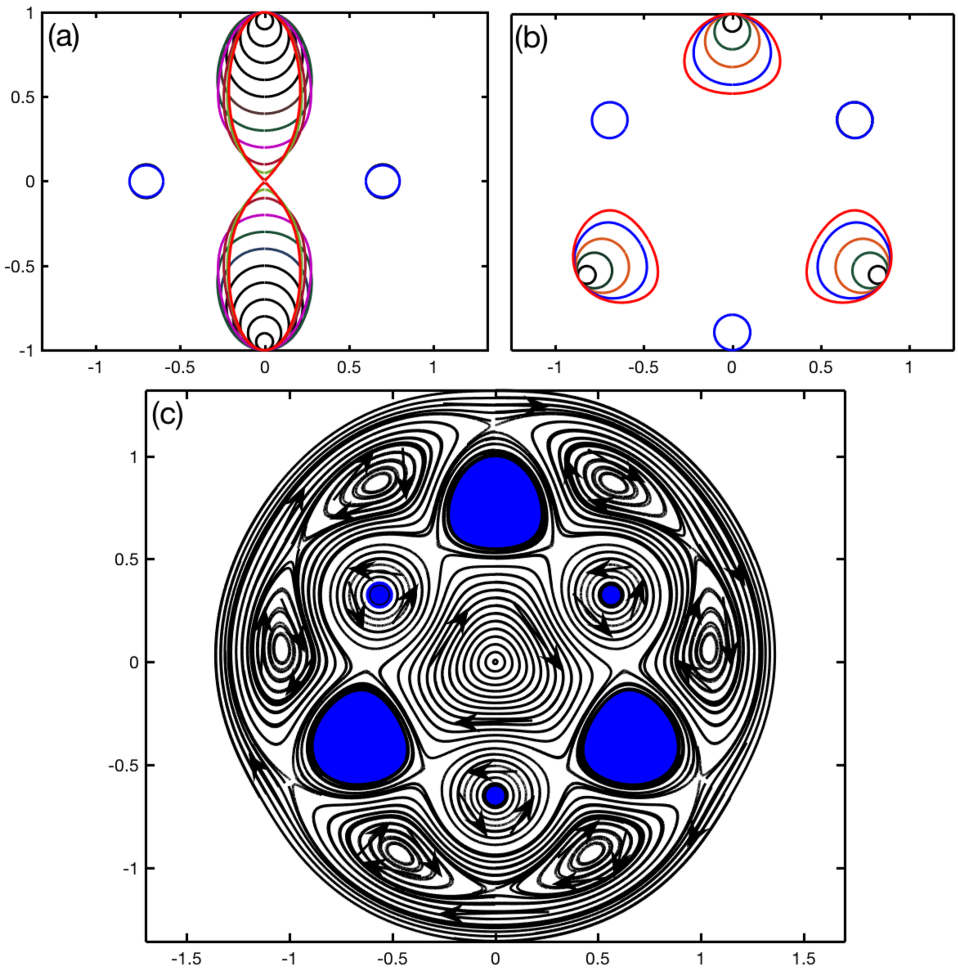

FIG. 15. Same-signed ($\alpha > 0$) staggered "$N + N$" equilibria. (a) "2 + 2" equilibria for $a_1 = 0.9, 0.8, 0.7, 0.6, 0.5, 0.4, 0.3, 0.2, 0.1, 0.05, 0.01$, $a_2 = 1$, $b_1 = 0.6$, $b_2 = 0.8$, $\omega_a = 1$ with $\omega_b = 0.53, 1.75, 3.31, 4.98, 6.58, 7.91, 8.59, 8.09, 6.37, 5.43, 5.10$. (b) "3 + 3" equilibria for $a_1 = 0.9, 0.8, 0.7, 0.6, 0.55$, $a_2 = 1$, $b_1 = 0.7$, $b_2 = 0.9$, $\omega_a = 1$ with $\omega_b = 0.31, 1.13, 2.41, 4.22, 5.50$. (c) Streamlines for a "3 + 3" equilibrium with $a_1 = 0.55$, $a_2 = 1$, $b_1 = 0.6$, $b_2 = 0.7$ giving $\omega_b = 24.6$. All shaded regions are vortex patches having same-signed vorticity.

3. The aligned "$N + N$" equilibria of either same-signed vorticity or opposite-signed vorticity are less stable than their staggered "$N + N$" equilibria counterparts.

The evolution of same-signed, aligned "$N + N$" equilibria for $N = 2, 3$ is shown in Fig. 17. In both the $N = 2, 3$ cases, the outer set of patches are drawn towards the inner set and merge to form a co-rotating pair ($N = 2$) and a tripolar ($N = 3$) rotating structure. However, for equilibria with the inner set of patches close to the origin, as shown in Fig. 18(a), they merge into a central patch. Figure 18(b) shows a similar unstable evolution for the "3 + 3" equilibrium with the inner set of patches merging to form a central patch When the two sets of patches are of comparable size and have boundaries not too different from circular as shown in Fig. 19 for a "3 + 3" equilibrium, the patches drift out of alignment and the inner patches contract radially towards the origin before returning to alignment with outer patches after which the inner patches rotate $2\pi/3$ relative to outer patches. This process occurs twice before the rotating structure is irreversibly destroyed ($t = 620$).

Recall that for opposite-signed, aligned "$N + N$" equilibria, only a limited range of solutions have been found. An opposite-signed equilibrium generally survives a relatively long time in terms of the turnover time for an individual vortex patch and is not shown here.

Staggered "$N + N$" equilibria are relatively more stable than aligned "$N + N$" equilibria. The same-signed, staggered "$N + N$" equilibria bear similar characteristics to the "$2N$"-polygon co-rotating equilibria. The "2 + 2" staggered equilibrium is the most unstable structure. Figure 20 shows the evolution of the same-signed "2 + 2" equilibrium when one set of polygonal patches, large and close to the origin, merge into a central patch, which is then eventually destroyed by the other set of patches. But the "$N + N$" configuration for $N \geq 3$ with centres of vorticities of each of the N patches of differing sizes lying on circles not far away from each other proves to be robust even when one set of patches are large and close to a limiting state. Figure 21 shows the evolution of a same-signed, staggered "4 + 4" equilibrium. Initially, the two sets of polygonal patches adjust radially with the smaller inner patches moving outwards and large outer patches contracting inwards such that the overall structure conserves angular momentum. The large patches are then drawn outwards when they get too close to the origin, and in the meantime, two polygonal patches rotate $\pi/2$ relative to the other. The smaller patches are then in turn drawn towards the origin while the larger set moves further away. After a second, similar, process, the larger patches undergo filamentation, which eventually destroys the rotating structure.

The opposite-signed staggered "$N + N$" equilibria with "comparable" sized patches are robust. When the outer set of

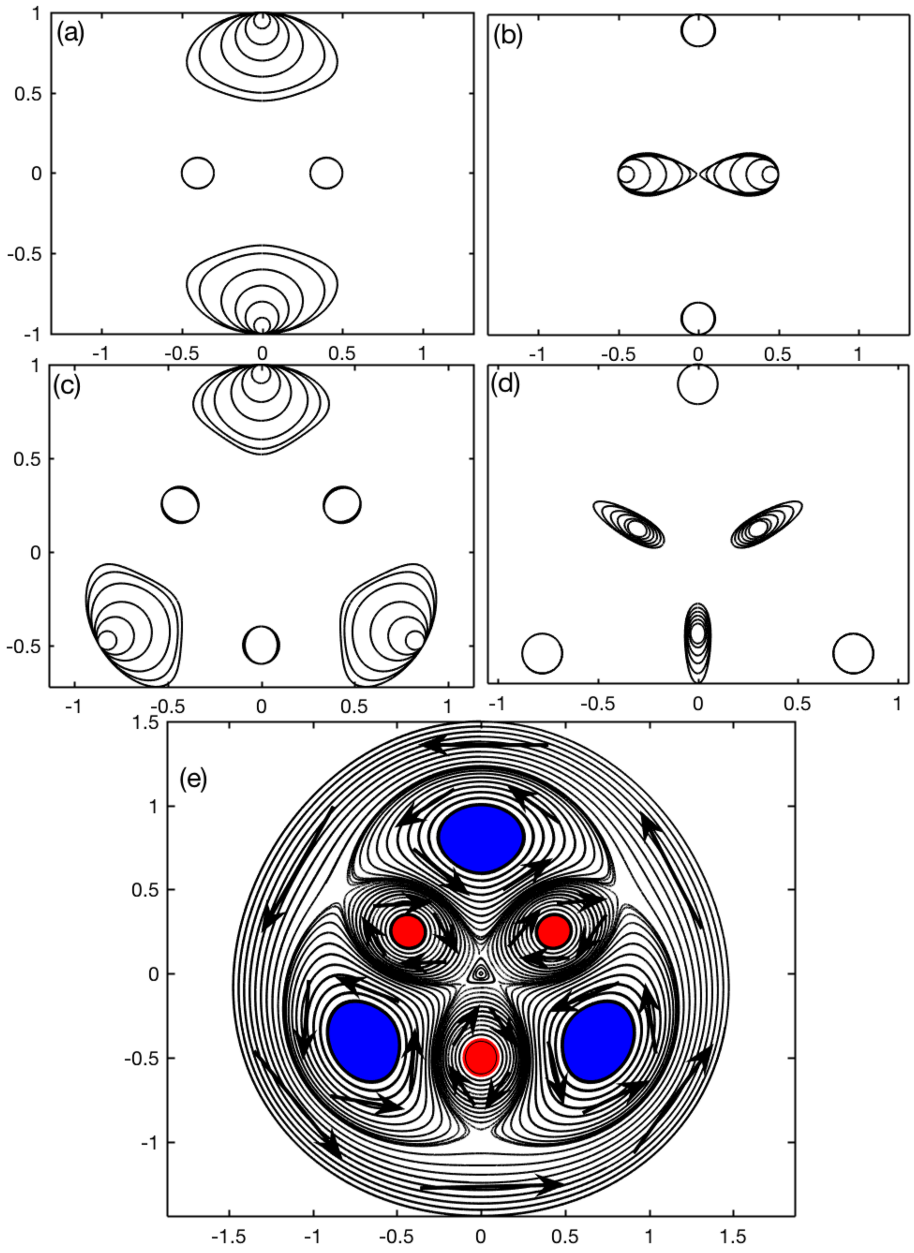

FIG. 16. Opposite-signed staggered "$N+N$" equilibria. (a) "2 + 2" equilibria for $a_1 = 0.9, 0.8, 0.7, 0.6, 0.5, 0.45$, $a_2 = 1$, $b_1 = 0.3$, $b_2 = 0.5$, $\omega_a = -1$ with $\omega_b = 0.28, 1.47, 4.74, 14.22, 47.93, 103.77$. (b) "2 + 2" equilibria for $a_1 = 0.8$, $a_2 = 1$, $b_1 = 0.4, 0.3, 0.2, 0.1, 0.05, 0.01$, $b_2 = 0.5$, $\omega_a = -1$ with $\omega_b = 11.73, 1.47, 0.42, 0.18, 0.14, 0.12$. (c) "3 + 3" equilibria for $a_1 = 0.9, 0.8, 0.7, 0.6, 0.55, 0.52$, $a_2 = 1$, $b_1 = 0.4$, $b_2 = 0.6$, $\omega_a = -1$ with $\omega_b = 0.11, 0.70, 2.97, 14.78, 45.13, 154.89$. (d) "3 + 3" equilibria for $a_1 = 0.8$, $a_2 = 1$, $b_1 = 0.2, 0.22, 0.24, 0.26, 0.28, 0.30$, $b_2 = 0.6, 0.55, 0.5, 0.46, 0.42, 0.4$, $\omega_a = -1$ with $\omega_b = 0.07, 0.07, 0.07, 0.07, 0.09, 0.15$. (e) Streamlines plot for a "3 + 3" equilibrium for $a_1 = 0.6$, $a_2 = 1$, $b_1 = 0.4$, $b_2 = 0.6$, $\omega_a = 1$ with $\omega_b = -14.78$. Shaded regions are vortex patches.

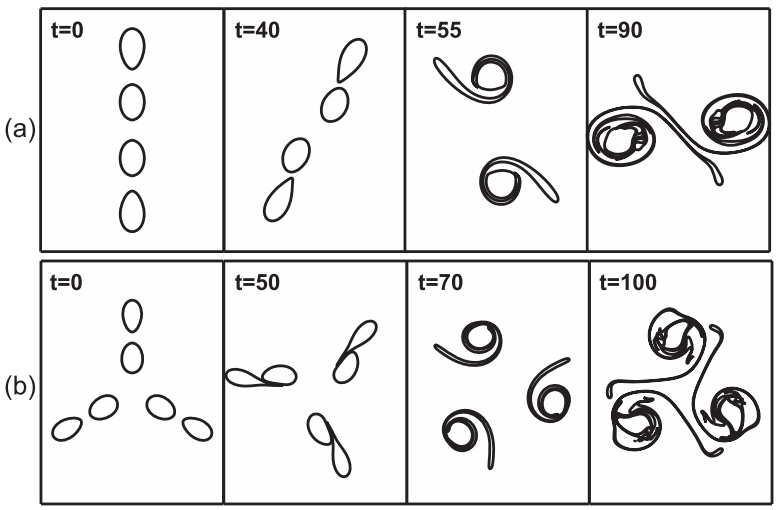

FIG. 17. Evolution of same-signed aligned "2 + 2" and "3 + 3" equilibrium. (a) "2 + 2" equilibrium with $a_1 = 0.6$, $a_2 = 1$, $b_1 = 0.1$, $b_2 = 0.45$, $\omega_a = 1$ giving a convergent $\omega_b = 1.55$. (b) "3 + 3" equilibrium with $a_1 = 0.65$, $a_2 = 1$, $b_1 = 0.2$, $b_2 = 0.53$ giving a value $\omega_b = 1.21$.

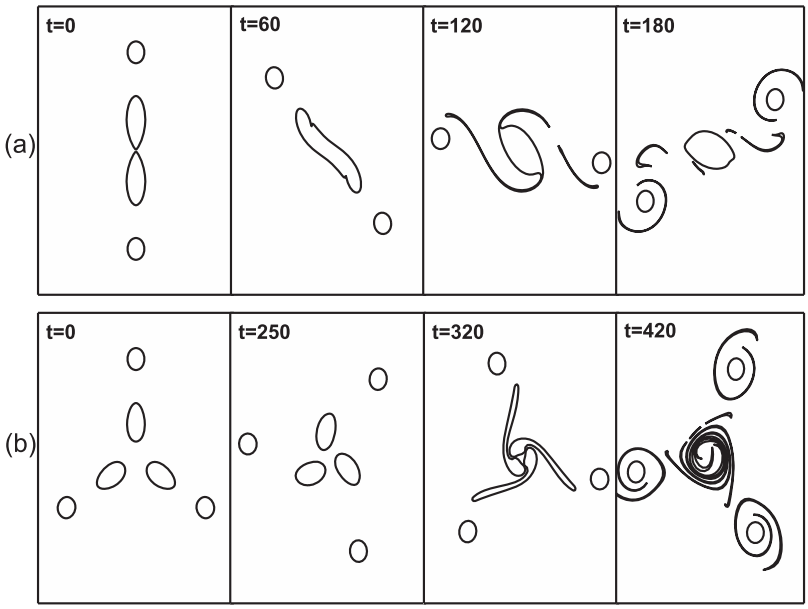

FIG. 18. Evolution of same-signed aligned "2 + 2" and "3 + 3" equilibrium. (a) "2 + 2" equilibrium with prescribed $a_1 = 0.8$, $a_2 = 1$, $b_1 = 0.01$, $b_2 = 0.5$, $\omega_a = 1$ giving a convergent $\omega_b = 0.28$. (b) "3 + 3" equilibrium with $a_1 = 0.8$, $a_2 = 1$, $b_1 = 0.15$, $b_2 = 0.5$, $\omega_a = 1$ giving a convergent $\omega_b = 0.25$.

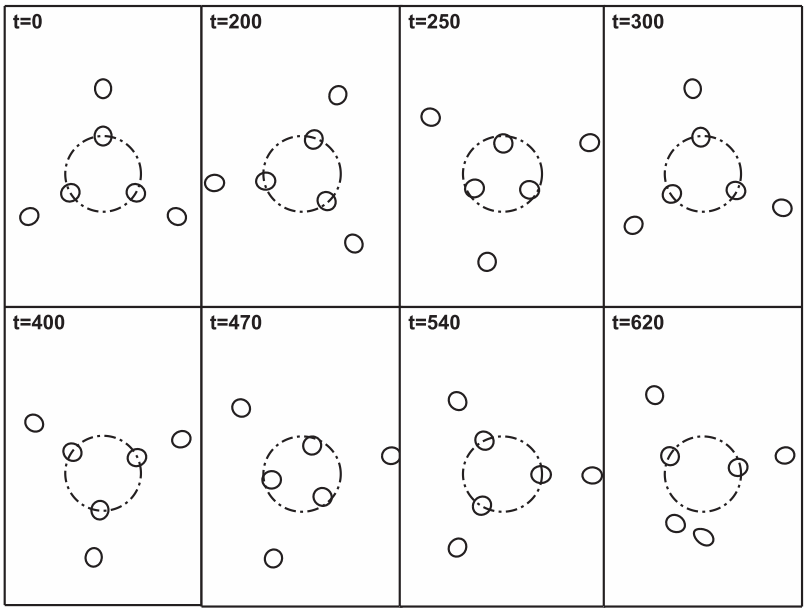

FIG. 19. Evolution of the same-signed aligned "3 + 3" equilibrium with $b_1 = 0.2$, $b_2 = 0.5$, $a_1 = 0.8$, $a_2 = 1$, $\omega_a = 1$ giving a convergent $\omega_b = 1.318$. Dashed-dotted circles indicate the radial drift of the inner set of patches.

polygonal patches are near the limiting states with scallop-like boundaries as in Figs. 16(a) and 16(c), these structures prove to be very robust since the scallop-like vortex patches are relatively weak in strength and stay firmly in their initial relative positions in the rotating structure. Near a limiting state, instability does eventually set in as shown in Fig. 22.

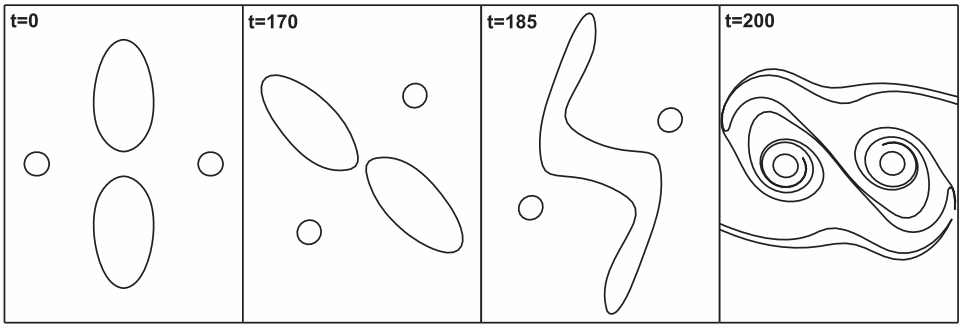

FIG. 20. Evolution of the same-signed, staggered "2 + 2" equilibrium with $b_1 = 0.6$, $b_2 = 0.8$, $a_1 = 0.1$, $a_2 = 1$, $\omega_a = 1$ with $\omega_b = 6.37$.

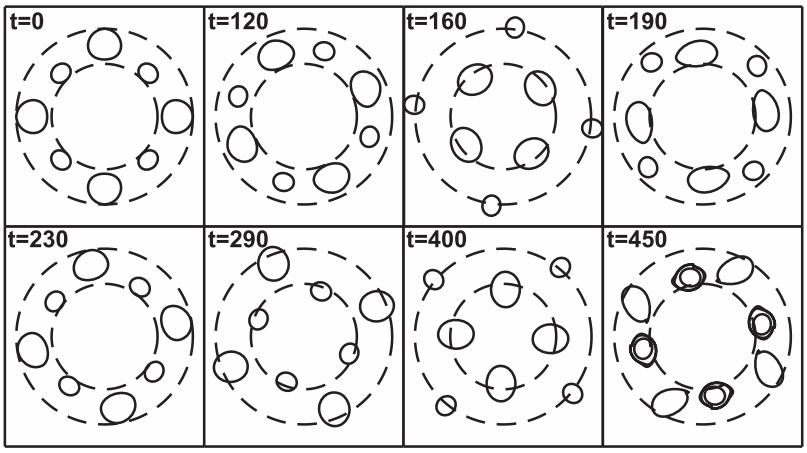

FIG. 21. Evolution of the same-signed staggered "4 + 4" equilibrium with prescribed $a_1 = 0.65$, $a_2 = 1$, $b_1 = 0.6$, $b_2 = 0.8$, $\omega_a = 1$ giving a convergent $\omega_b = 1.95$.

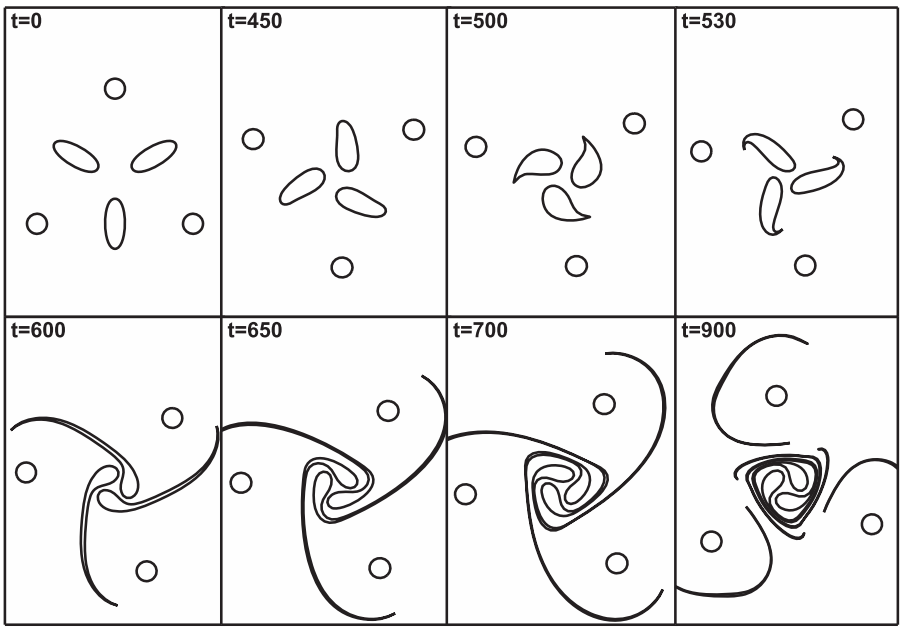

FIG. 22. Evolution of the opposite-signed staggered "3 + 3" equilibrium with $b_1 = 0.2$, $b_2 = 0.7$, $a_1 = 0.8$, $a_2 = 1$, $\omega_a = 1$, and $\omega_b = -0.09$.

V. SUMMARY AND DISCUSSION

Two distinct families of solutions have been computed for "N + 1" point vortex-vortex patch equilibria, i.e., same-signed equilibria and opposite-signed equilibria. The families have limiting states in which the central patch acquires tips or corners. Linear stability analysis shows that the central patch is most unstable near these limiting states.

The "N + 1" multipolar vortex equilibria, where finite-area satellite patches replace the point vortices, bear many similar properties of the "N + 1" point vortex-vortex patch equilibria. Two extra limiting behaviours exist when the satellite patches form tips. Time-dependent simulations of these multipolar vortex equilibria show that opposite-signed equilibria are more stable structures relative to their same-signed counterparts. Various forms of instability are evident including filamentation at tips and corners and vortex pairing to form either same-signed or opposite-signed (propagating) dipoles. In comparison to the "N + 1" point vortex equilibria, it has been shown that the finite area of the satellite patches plays an important role in the stability of vortex equilibria. In a "N + 1" multipolar vortex equilibrium, a relatively weak central patch is most susceptible to filamentation and distortion as well as breaking. Increasing the number of satellite patches suppresses the central patch instability but introduces circular instability of the satellite patches especially in opposite-signed equilibria. The circular instability is suppressed in a same-signed "N + 1" multipolar equilibrium due to the opposing flow between the central and satellite patches.

The "N + N" nested polygonal equilibria consist of aligned or staggered arrangement of vortex patches, each having same-signed and opposite-signed solutions. Various limiting shapes have been found along with their streamlines. These equilibria are typically less stable than the "N + 1" multipolar equilibria. In some solution regimes, time-dependent integrations have shown that the nested polygonal equilibria evolve into "N + 1" vortex equilibria. The same-signed aligned polygonal equilibria are less stable than staggered equilibria and frequently evolve into N-polygon co-rotating structures. The opposite-signed aligned "N + N" equilibria have complex flow fields, and only a limited range of equilibria have been found. A typical instability mechanism of such

equilibria results in opposite-signed vortex patches pairing up and propagating away from their initial location. The staggered polygonal equilibria are more robust structures. Same-signed staggered "$N + N$" equilibria are similar to the $2N$-polygonal equilibria. The opposite-signed staggered polygonal equilibria survive for longer times in time-dependent evolution, but those near limiting states undergo vortex merging, breaking, and filamentation.

ACKNOWLEDGMENTS

B.B.X was supported by a UK Engineering and Physical Sciences Research Council (EPSRC) Ph.D. studentship, Grant No. EP/L504889/1.

APPENDIX A: WOZ NUMERICAL ROUTINE

Assume the boundary points (x, y) of a vortex patch in an equilibrium configuration are expressed in polar coordinates relative to its "centre," e.g., centre of mass,

$$(x - x_0, y - y_0) = R(\theta)(\cos\theta, \sin\theta), \tag{A1}$$

where (x_0, y_0) is the "centre" of the vortex. The boundary condition in (2) can be written as

$$u\frac{\mathrm{d}y}{\mathrm{d}\theta} - v\frac{\mathrm{d}x}{\mathrm{d}\theta} + \Omega\widetilde{R}\frac{\mathrm{d}\widetilde{R}}{\mathrm{d}\theta} = 0, \tag{A2}$$

where $\widetilde{R}$ is the distance of the patch boundary point to the origin, which is equal to R if the vortex is centred at the origin (monopole). Note that

$$\begin{aligned}\widetilde{R}^2 &= (R\cos\theta + x_0)^2 + (R\sin\theta + y_0)^2 \\ &= R^2 + 2R\cos\theta x_0 + 2R\sin\theta y_0 + x_0^2 + y_0^2.\end{aligned} \tag{A3}$$

The contour dynamics routine gives (u_k, v_k), $k = 1, 2, \ldots, K$, where K is the total number of discretized points on all patches and the velocities

$$(u_k, v_k) = \frac{1}{2\pi}\sum_{j=1}^{\widetilde{N}}\omega_j\sum_{i=1}^{N_T^{(j)}}\frac{\left(x_k - \xi_{i+1/2}^{(j)}, y_k - \eta_{i+1/2}^{(j)}\right)}{\left[\left(x_k - \xi_{i+1/2}^{(j)}\right)^2 + \left(y_k - \eta_{i+1/2}^{(j)}\right)^2\right]^{1/2}}\left(l_{k,i+1}^{(j)} - l_{k,i}^{(j)}\right), \tag{A4}$$

where ω_j is the vorticity of the ith vortex patch, $\widetilde{N}$ is the total number of vortex patches in the equilibrium, $N_T^{(j)}$ is the total number of points on the jth vortex patch, $f_{i+1/2} = (f_i + f_{i+1})/2$, $\left(\xi_i^{(j)}, \eta_i^{(j)}\right) \in \partial D_j$, and

$$l_{k,i}^{(j)} = \left[\left(x_k - \xi_{i+1/2}^{(j)}\right)^2 + \left(y_k - \eta_{i+1/2}^{(j)}\right)^2\right]^{1/2}. \tag{A5}$$

For the computation of the N-fold symmetric monopolar equilibrium, Fig. 23 shows $M + 1$ boundary points with R_1 and R_{M+1} fixed and R_k adjustable at each iteration. With second order accuracy, the boundary condition in (A2) is expressed as

$$u_{k+1/2}\Delta y_k - v_{k+1/2}\Delta x_k + (\Omega/2)\Delta\widetilde{R}_k^2 = 0, \quad 1 \le k \le M, \tag{A6}$$

where $\Delta f_k = f_{k+1} - f_k$ and $u_{k+1/2} = (u_k + u_{k+1})/2$. Substituting (A3) into (A6) gives

$$\begin{aligned}&u_{k+1/2}\Delta(R_k\sin\theta_k) - v_{k+1/2}\Delta(R_k\cos\theta_k) \\ &\quad + (\Omega/2)\left(\Delta R_k^2 + 2\Delta R_k\cos\theta_k x_0 + 2\Delta R_k\sin\theta_k y_0\right) = 0.\end{aligned} \tag{A7}$$

Using (A1), then (A7) is reduced to

$$R_k - F_{k+1/2}R_{k+1} = 0, \qquad 1 \le k \le M, \tag{A8}$$

or, alternatively,

$$R_k - F_{k-1/2}^{-1}R_{k-1} = 0, \qquad 2 \le k \le M + 1, \tag{A9}$$

where the function $F_{k+1/2}$ is defined as

$$F_{k+1/2} = \frac{u_{k+1/2}\sin\theta_{k+1} - v_{k+1/2}\cos\theta_{k+1} + (\Omega/2)R_{k+1} + \Omega x_0\cos\theta_{k+1} + \Omega y_0\sin\theta_{k+1}}{u_{k+1/2}\sin\theta_k - v_{k+1/2}\cos\theta_k + (\Omega/2)R_k + \Omega x_0\cos\theta_k + \Omega y_0\sin\theta_k}. \tag{A10}$$

Now a three-point scheme and a relaxation procedure follow: first average (A8) and (A9) to give

$$-\frac{1}{2}F_{k-1/2}^{-1}\bar{R}_{k-1} + \bar{R}_k - \frac{1}{2}F_{k+1/2}\bar{R}_{k+1} = 0, \qquad 2 \le k \le M, \tag{A11}$$

where $\bar{R}_1 = a_1$, $\bar{R}_{M+1} = a_2$ are prescribed and fixed. Equation (A11) can then be used to solve for $\bar{R}_k$ given $F_{k+1/2}$. Assume $R_k^{(n)}$ are the boundary points after the nth iteration. The velocities are found using second order discretization, and Ω is updated by summing (A6), giving

$$\Omega^{(n)} = 2\sum_{k=1}^{M}\left[u_{k+1/2}^{(n)}\Delta y_k^{(n)} - v_{k+1/2}^{(n)}\Delta x_k^{(n)}\right]/\left(\widetilde{R}_1^2 - \widetilde{R}_{M+1}^2\right). \tag{A12}$$

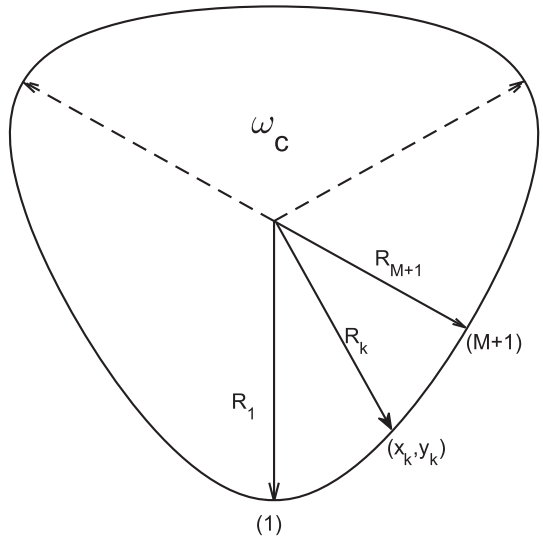

FIG. 23. Discretization of the boundary of a N-fold symmetry vortex patch. Here $N = 3$. By symmetry, only a $1/2N$ section of the boundary needs to be considered. That is, R_k for $1 \le k \le M + 1$ with corresponding $0 \le \theta_k + \pi/2 \le \pi/N$. Here $M + 1$ is the number of points on that section of the boundary.

This in turn gives $F^{(n)}_{k+1/2}$ and can be used to solve for $R^{(n+1)}_k$. Finally a relaxation is used,

$$R^{(n+1)}_k = \mu \bar{R}^{(n+1)}_k + (1-\mu) R^{(n)}_k, \tag{A13}$$

where μ is the relaxation parameter. This completes an iteration. This iteration continues until

$$||R^{(n+1)}_k - R^{(n)}_k|| < 10^{-6}. \tag{A14}$$

APPENDIX B: MODIFIED WOZ METHOD FOR "*N* + 1" POINT VORTEX-VORTEX PATCH EQUILIBRIA

Two routines are described below for the "$N + 1$" point vortex-vortex patch equilibrium shown in Fig. 1(a). For all the computations, at least 300 points are used on each symmetric section of an individual patch.

1. Prescribing only one characteristic radius of central patch

To find the convergent solution uniquely defined by R_1, b, ω_c, Γ_s, the boundary points on a $1/N$ section of the central patch need to be considered using the procedure described in Appendix A, i.e., the boundary points R_k for $1 \le k \le 2M + 1$ in Fig. 1(a) where $R_1 = R_{2M+1} = a_1$ are prescribed. A circular patch is used to initialise the computation. The rotational velocity Ω cannot be updated using (A12) since $R_1 = R_{2M+1}$. Instead, it is updated using the boundary condition that the point vortex is fixed in the rotating frame,

$$u\left(\omega_c, \Gamma_s, b, x^{(n)}_k, y^{(n)}_k\right) + \Omega^{(n+1)} b = 0$$

or

$$\Omega^{(n+1)} = u\left(\omega_c,\ \Gamma_s,\ b,\ \underline{x}^{(n)},\ \underline{y}^{(n)}\right)/b, \tag{B1}$$

where u is the velocity at the point vortex and $\underline{x}^{(n)} = \left(x^{(n)}_1, x^{(n)}_2, \ldots, x^{(n)}_K\right)$ are the boundary points at the nth iteration. The procedure now follows that of Appendix A.

2. Prescribing two characteristic radii of central patch

An alternative is to find a convergent solution by prescribing R_1, R_{M+1}, b, and ω_c. This means that the strength of the satellite point vortices Γ_s need to be determined as part of the solution. The boundary points that need to be updated are R_k for $1 \le k \le M + 1$ with $R_1 = a_1$ and $R_{M+1} = a_2$. At the nth iteration with $\left(x^{(n)}_k, y^{(n)}_k\right)$, the boundary condition from (A12) and (B1) gives two linear equations for Ω and Γ_s. The velocities are split into two parts: a contribution from the central patch and a contribution from point vortices as follows:

$$\begin{aligned}\omega_c \sum_{k=1}^{M} \left[u^{(cc)}_{k+1/2}\Delta y^{(n)}_k - v^{(cc)}_{k+1/2}\Delta x^{(n)}_k\right] \\ + \frac{\Gamma^{(n+1)}_s}{2\pi} \sum_{k=1}^{M} \left[u^{(cp)}_{k+1/2}\Delta y^{(n)}_k - v^{(cp)}_{k+1/2}\Delta x^{(n)}_k\right] \\ + \frac{\Omega^{(n+1)}}{2}\left(R^2_{M+1} - R^2_1\right) = 0,\end{aligned} \tag{B2}$$

$$\omega_c u^{(pc)} + \frac{\Gamma^{(n+1)}_s}{2\pi} u^{(pp)} + \Omega^{(n+1)} b = 0, \tag{B3}$$

where $u^{(cc)}_{k+1/2}$ is the velocity on the central patch boundary points induced by the central patch, $u^{(cp)}_{k+1/2}$ is the velocity on the central patch due to the surrounding point vortices of unit strength, $u^{(pc)}$ is the velocity at the point vortex induced by the unit strength central patch, and $u^{(pp)}$ is the velocity at the point vortex owing to the other point vortices. The coupled linear equations (B2) and (B3) are solved to find $\Omega^{(n+1)}$, $\Gamma^{(n+1)}_s$, enabling $F_{k+1/2}$ to be found. Finally, the initial profile for the central patch to initialise computation is

$$R = \frac{1}{2}(a_1 + a_2) + \frac{1}{2}(a_1 - a_2)\cos(N(\theta + \pi/2)). \tag{B4}$$

APPENDIX C: NUMERICAL ROUTINE FOR FINDING "*N* + 1" MULTIPOLAR VORTEX EQUILIBRIA

Equilibria sought by prescribing a_1, a_2, b_1, b_2, and ω_c mean that ω_s has to be determined. The central and satellite patches are discretized with boundary points R^c_k, $2 \le k \le M$, and R^s_k, $2 \le k \le P$, respectively, such that boundary points are evenly spaced θ in polar coordinates. $R^c_1, R^c_{M+1}, R^s_1, R^s_{P+1}$ are fixed. These radii are defined relative to the relevant patch "centre," which is taken to be the origin for the central patch and the radial midpoint of the satellite patches. An initial boundary profile in the form of (B4) is used for the central patch, and a circle is used for satellite patches. The corresponding modifications for updating the boundary points are given in Appendix A, the difference here being that there are two functions $F^c_{k+1/2}$ and $F^s_{k+1/2}$ defined as in (A10) for two sets of boundary points which are used in (A11) to update boundary points. In order to find $F^c_{k+1/2}$ and $F^s_{k+1/2}$, at the nth iteration, the vorticity ω_s and Ω are updated using boundary conditions (A12) on two separate boundaries. These two equations are coupled linear equations in ω_s and Ω, and after splitting the velocities due to the contribution of different patches, they

give

$$\omega_c \sum_{k=1}^{M+1} [u^{(cc)}_{k+1/2}\Delta y^c_k - v^{(cc)}_{k+1/2}\Delta x^c_k] + \omega_s \sum_{k=1}^{M+1} [u^{(cs)}_{k+1/2}\Delta y^c_k - v^{(cs)}_{k+1/2}\Delta x^c_k] = \frac{\Omega}{2}(a_1^2 - a_2^2),$$
$$\omega_c \sum_{k=1}^{P+1} [u^{(sc)}_{k+1/2}\Delta y^s_k - v^{(sc)}_{k+1/2}\Delta x^s_k] + \omega_s \sum_{k=1}^{P+1} [u^{(ss)}_{k+1/2}\Delta y^s_k - v^{(ss)}_{k+1/2}\Delta x^s_k] = \frac{\Omega}{2}(b_1^2 - b_2^2), \quad \text{(C1)}$$

where $(x^c_k, y^c_k), (x^s_k, y^s_k)$ are the boundary points on the central and satellite patches. (C1) is solved for ω_s, Ω.

The same procedure can be applied to find equilibria with more than two sets of identical vortex patches by prescribing two characteristic radial points of each patch along with the vortex strength of one of the patch sets. For example, with 3 sets of patches in an equilibrium, three sections of boundary points need to be considered and correspondingly three $F_{k+1/2}$ for each boundary must be computed. The equivalent of (C1) then becomes three linear equations in the vorticity strengths of two other sets of vortex patches and Ω.

[1] J. J. Thomson, *A Treatise on the Motion of Vortex Rings: An Essay to which the Adams Prize was Adjudged in 1882, in the University of Cambridge* (Macmillan, 1883).
[2] H. Aref, "Point vortex motions with a center of symmetry," Phys. Fluids **25**, 2183–2187 (1982).
[3] H. Aref, P. K. Newton, M. A. Stremler, T. Tokieda, and D. L. Vainchtein, "Vortex crystals," Adv. Appl. Mech. **39**, 1–79 (2003).
[4] H. Lamb, *Hydrodynamics* (Cambridge University Press, 1932).
[5] A. E. H. Love, "On the stability of certain vortex motions," Proc. London Math. Soc. **s1–25**, 18–43 (1893).
[6] Y. Tang, "Nonlinear stability of vortex patches," Trans. Am. Math. Soc. **304**, 617–638 (1987).
[7] H. M. Wu, E. A. Overman, and N. J. Zabusky, "Steady-state solutions of the Euler equations in two dimensions: Rotating and translating V-states with limiting cases. I. Numerical algorithms and results," J. Comput. Phys. **53**, 42–71 (1984).
[8] R. T. Pierrehumbert, "A family of steady, translating vortex pairs with distributed vorticity," J. Fluid Mech. **99**, 129–144 (1980).
[9] G. S. Deem and N. J. Zabusky, "Vortex waves: Stationary 'V states,' interactions, recurrence, and breaking," Phys. Rev. Lett. **40**, 859–862 (1978).
[10] E. A. Overman II, "Steady-state solutions of the Euler equations in two dimensions II. Local analysis of limiting V-states," SIAM J. Appl. Math. **46**, 765–800 (1986).
[11] P. G. Saffman and S. Tanveer, "The touching pair of equal and opposite uniform vortices," Phys. Fluids **25**, 1929–1930 (1982).
[12] J. Burbea, "On patches of uniform vorticity in a plane of irrotational flow," Arch. Ration. Mech. Anal. **77**, 349–358 (1981).
[13] D. G. Crowdy, "Exact solutions for rotating vortex arrays with finite-area cores," J. Fluid Mech. **469**, 209–235 (2002).
[14] P. G. Saffman and R. Szeto, "Equilibrium shapes of a pair of equal uniform vortices ," Phys. Fluids **23**, 2339–2342 (1980).
[15] D. G. Dritschel, "The stability and energetics of corotating uniform vortices," J. Fluid Mech. **157**, 95–134 (1985).
[16] P. K. Newton, *The N-Vortex Problem: Analytical Techniques* (Springer Science & Business Media, 2013), Vol. 145.
[17] V. D. Larichev and G. M. Reznik, "Collision of two-dimensional solitary Rossby waves," Okeanologiya **23**, 725–734 (1983).
[18] J. B. Flór, W. S. S. Govers, G. J. F. Van Heijst, and R. Van Sluis, "Formation of a tripolar vortex in a stratified fluid," in *Advances in Turbulence IV* (Springer, 1993), pp. 405–409.
[19] B. Legras, P. Santangelo, and R. Benzi, "High-resolution numerical experiments for forced two-dimensional turbulence," Europhys. Lett. **5**, 37 (1988).
[20] G. J. F. Van Heijst, R. C. Kloosterziel, and C. W. M. Williams, "Laboratory experiments on the tripolar vortex in a rotating fluid," J. Fluid Mech. **225**, 301–331 (1991).
[21] G. F. Carnevale and R. C. Kloosterziel, "Emergence and evolution of triangular vortices," J. Fluid Mech. **259**, 305–331 (1994).
[22] V. G. Makarov, "Numerical simulation of the formation of tripolar vortices by the method of contour dynamics," Izv. Atmos. Ocean Phys. **32**, 40–49 (1996).
[23] Z. Kizner and R. Khvoles, "The tripole vortex: Experimental evidence and explicit solutions," Phys. Rev. E **70**, 016307 (2004).
[24] A. Okamoto, K. Hara, K. Nagaoka, S. Yoshimura, J. Vranješ, M. Kono, and M. Y. Tanaka, "Experimental observation of a tripolar vortex in a plasma," Phys. Plasmas **10**, 2211–2216 (2003).
[25] J. Vranješ, G. Marić, and P. K. Shukla, "Tripolar vortices and vortex chains in dusty plasma," Phys. Lett. A **258**, 317–322 (1999).
[26] Z. Kizner, R. Khvoles, and J. C. McWilliams, "Rotating multipoles on the f-and γ-planes," Phys. Fluids **19**, 016603 (2007).
[27] L. M. Polvani and X. J. Carton, "The tripole: A new coherent vortex structure of incompressible two-dimensional flows," Geophys. Astrophys. Fluid Dyn. **51**, 87–102 (1990).
[28] Y. G. Morel and X. J. Carton, "Multipolar vortices in two-dimensional incompressible flows," J. Fluid Mech. **267**, 23–51 (1994).
[29] P. G. Saffman, *Vortex Dynamics* (Cambridge University Press, 1992).
[30] L. J. Campbell, "Transverse normal modes of finite vortex arrays," Phys. Rev. A **24**, 514 (1981).
[31] H. Aref, "A transformation of the point vortex equations," Phys. Fluids **14**, 2395–2401 (2002).
[32] X. J. Carton, "On the merger of shielded vortices," Europhys. Lett. **18**, 697 (1992).
[33] X. J. Carton, G. R. Flierl, and L. M. Polvani, "The generation of tripoles from unstable axisymmetric isolated vortex structures," Europhys. Lett. **9**, 339 (1989).
[34] X. Carton and B. Legras, "The life-cycle of tripoles in two-dimensional incompressible flows," J. Fluid Mech. **267**, 53–82 (1994).
[35] G. K. Morikawa and E. V. Swenson, "Interacting motion of rectilinear geostrophic vortices," Phys. Fluids **14**, 1058–1073 (1971).
[36] J. N. Reinaud, M. A. Sokolovskiy, and X. Carton, "Geostrophic tripolar vortices in a two-layer fluid: Linear stability and nonlinear evolution of equilibria," Phys. Fluids **29**, 036601 (2017).
[37] B. Shteinbuch-Fridman, V. Makarov, X. Carton, and Z. Kizner, "Two-layer geostrophic tripoles comprised by patches of uniform potential vorticity," Phys. Fluids **27**, 036602 (2015).
[38] M. A. Sokolovskiy, J. Verron, and O. I. Yakovenko, *Dynamics of Vortex Structures in a Stratified Rotating Fluid* (Springer, 2014).
[39] D. G. Dritschel, "The nonlinear evolution of rotating configurations of uniform vorticity," J. Fluid Mech. **172**, 157–182 (1986).
[40] D. G. Dritschel, "Contour surgery: A topological reconnection scheme for extended integrations using contour dynamics," J. Comput. Phys. **77**, 240–266 (1988).
[41] D. Crowdy and J. Marshall, "Growing vortex patches," Phys. Fluids **16**, 3122–3130 (2004).